ISSN 0915-6348

NATIONAL INSTITUTE FOR FUSION SCIENCE

Proceedings of JSPS-CAS Core University Program Seminar on Target Materials, July 28 - Aug. 1, 2007, Huangshan, Anhui

(Eds.) Z.Z. Gu and T. Norimatsu

(Received - Aug. 15, 2007)

NIFS-PROC-70 Feb. 2008

RESEARCH REPORT
NIFS-PROC Series

TOKI, JAPAN

Proceeding of JSPS-CAS Core University Program Seminar on Target Materials

Z. Z. Gu, T. Norimatsu Eds.

July 28-Aug.1,2007

Huangshan, Anhui

JSPS-CAS Core University Program Seminar on Target Materials

Organized by: State Key Laboratory of Bioelectronics, Southeast University
Institute of Laser Engineering, Osaka University
Research Center of Laser Fusion, CAEP

Foreword:

China-Japan Bilateral Collaboration on the Study of Ultrahigh Density Plasma has been established since 2001 and its second phase is conducting from 2006. Target materials are key issue of the Study of Ultrahigh Density Plasma, and the section of target fabrication was opened at the 2005 Workshop on Ultrahigh Density Plasma Production, Application and theory for Laser Fusion at Nine Village Valley, Sichuan. It achieved great successes in high-level academic exchange and efficient presentation of state-of –the –art development in this research field. However, in order to attract greater attention and participation of more scientists in these fields, the organizing committee decided to further specify and enlarge the scale of the workshop to be China-Japan Bilateral Seminar on Target Materials 2007 in Huang Shan in southern Anhui Province of east China. The seminar had more than 20 participants from 7 universities and 3 institutes in Japan and China. They exchanged state-of-the-art development in nanomaterials, capsule fabrication and low density materials toward target of high power laser.

Keywords:

Laser Plasma Targets, Low Density Materials, Capsules Fabrication and Applications, Cryogenic Targets, Photoenergy Conversion Materials, Nanomaterials, Surface Modification, Nanoassembly, Photo-functional Materials, Electrochemistry, Target Injection and Tracking

Committees

Chairmen:

Zhongze Gu (Southeast Univ.), Yongjian Tang (CAEP)

Takayoshi Norimatsu (Osaka Univ.), Keiji Nagai (Osaka Univ.)

Committee Members:

China: Weiyan Zhang (CAEP)

Yongkun Ding (CAEP)

Ling Zhan (CAEP)

Bo Li (CAEP)

Weidong Wu (CAEP)

Guangming Li (Heilongjiang Univ.)

Jianyu Zheng (Nankai Univ.)

Baopin Ling (Southeast Univ.)

Xiangwei Zhao (Southeast Univ.)

Japan:

H. Homma (Osaka Univ.)

A. Iwamoto (National Inst. Fusion Sci.)

T. Mito (National Inst. Fusion Sci.)

M. Nakai (Osaka Univ.)

N. Nemoto (Nihon Univ.)

K. Takato (Tsukuba Gakuin Univ.)

M. Yagi (Niigata Univ.)

H. Yoshida (Gifu Univ.)

Main Theme of JSPS-CAS Core University Program

Seminar on Target Materials 2007

1) Laser Plasma Targets
2) Low Density Materials
3) Capsules Fabrication and Applications
4) Cryogenic Targets
5) Photoenergy Conversion Materials
6) Nanomaterials
7) Surface Modification, Nanoassembly
8) Photo-functional Materials
9) Electrochemistry
10) Target Injection and Tracking
11) Others

CONTENTS

Ⅰ.Plenary Lectures

Ⅱ.Invited Reports

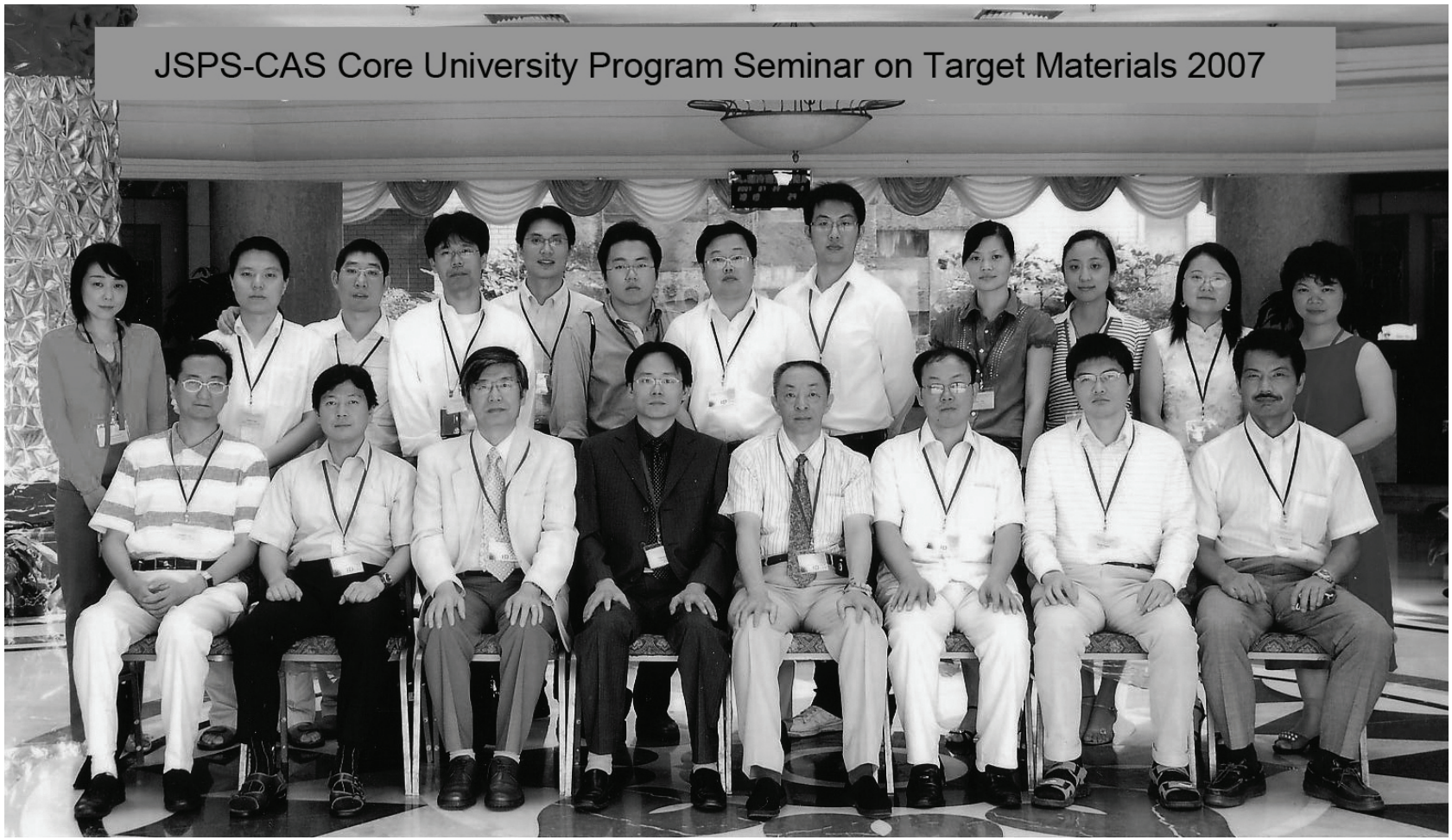
JSPS-CAS Core University Program Seminar on Target Materials 2007

Application of Nanotechnology in Laser Inertial Confinement Fusion

Yong-Jian Tang*

Research Center of Laser Fusion, China Academy of Engineering Physics, P. O. Box 919-987, Mianyang, Sichuan, China

Abstract: The achievements of nanotechnology applied in designing and processing laser inertial confinement fusion targets as well as in measuring laser-plasma irradiation energy spectra in the past 15 years in Research Center of Laser Fusion in China are reported in this paper.

Introduction

Laser inertial confinement fusion (ICF) is an alternative way to achieve controlled thermonuclear fusion. The basic elements of ICF include drivers and targets, covering precise diagnosis, target design and high power laser. The success of an ICF experiment based on large and complex facilities depends largely on the size, components and structure of tiny ICF targets. Therefore, research on design, production, and characterization of ICF targets has become an integral part of work in the Research Center of Laser Fusion (RCLF) in China and other institutes all over the world. Although the laser system providing energy may be as large as a football field, the ICF targets should not be made too large due to the power density limitation of laser equipments, and generally a target containing fusion fuel is only several millimeters in diameter or even smaller. Consequently, the units in the target must be smaller than a micrometer. Based on this fact, scientists have begun to turn to nanotechnology for improving performance of the targets. In the past 15 years, nanotechnology has been applied in designing and processing ICF targets as well as measuring laser-plasma irradiation energy spectra. Since 1993, various research subjects such as nanofilms, nanopowders, and nanofoams have been involved in the RCLF of China. Thereinafter we will introduce some research results on these fields.

Nanofoams

Nanostructured Cu and Au porous foams (as shown in Fig.1(a)) with density only 0.5~10% of the bulk metals have been successfully made by vapor-phase deposition (VPD) [1]. In 1995, Wang *et al* produced low-density polystyrene (PS), resorcinol formaldehyde (RF), and carbonized resorcinol formaldehyde (CRF) foams [2]. The density of these foams ranges from 15 mg/cm^3 to 1000 mg/cm^3, the fraction of pores can reach 80~99.8%, the typical pore size is within 1~50 nm, and the ratio surface area reaches 200~1000 m^2/g. Fig.1(b) shows a typical transmission electron microscopy (TEM) image of the carbonized RF arogel foams, whose skeleton and pores are both below 10 nm in diameter. These foams have been used to study storage of hydrogen.

*Email: tangyongjian2000@sina.com

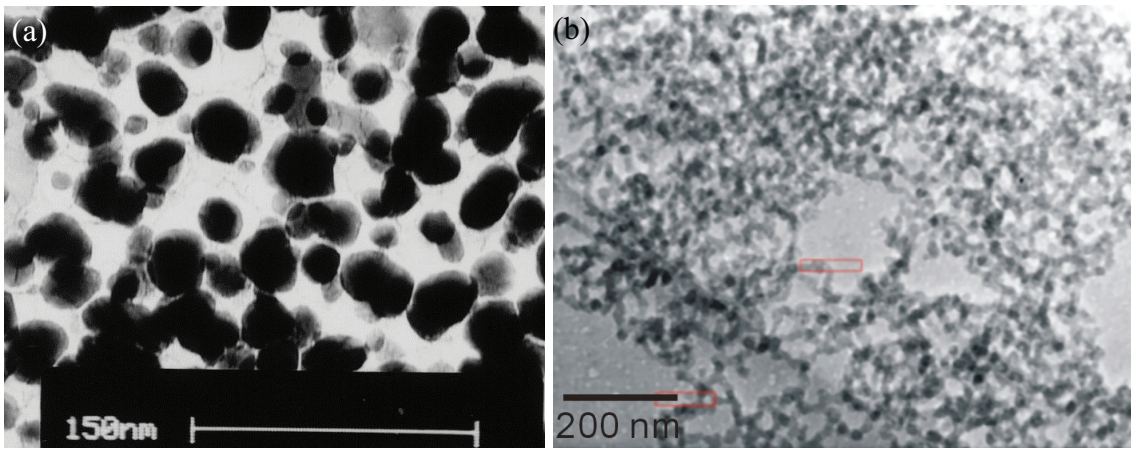

Fig.1 TEM images of (a) Au foams and (b) carbonized RF aerogel foams.

In 1999, Zhang et al synthesized pure poly-4-methyl-1-pentene (PMP) foams, which might be the lightest in China, with density of 1-50 mg/cm^3, density uniformity larger than 90% and pore size of 20~10000 nm [3]. The synthesis process involved solving the PMP resource in solvents at high temperature, then cooling the solution at certain rate to form a gel, finally drying the gel by vacuum sublimation to obtain porous foams with interconnecting voids. The porous PMP foams were doped with Cl, Br, and Cu, of which the density was lower than 50 mg/cm^3 and the mass fraction of dopants was below 1%. Fig.2(a) to (c) show the machined PMP foams doped with Cl, Br, and Cu respectively.

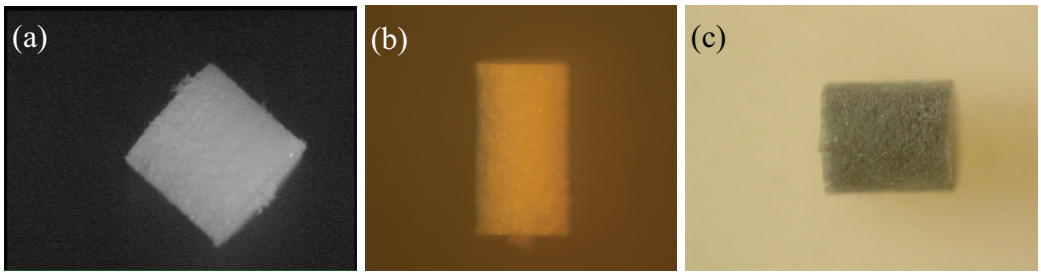

Fig.2 Photos of machined PMP foams doped with (a) Cl, (b) Br, and (c) Cu.

Nanofilms

By studying the process of fabricating modified polystyrene, a set of equipment (Langmuir-Blodgett film tank system) for producing ultrathin film was built. Ultrathin and unsupported PS film with thickness below 50 nm was grown [4]. Molecule-beam-levitation, supersonic-levitation, and electromagnetic-vibration technologies were developed for 4π-rotation deposition of multilayer films. With these technologies, thickness of the deposited films can be controlled in the range from tens of nm to 100 μm. Organic films with micro and submicro structure were also fabricated, of which the thickness was from several to tens of microns. By investigating the process of inflating high-Z gas into hollow glass microspheres, a breakthrough was achieved in the aspect of implantation technique with short-wavelength laser, ion beam, and atomic force microscopy (AFM) drilling. In particular, AFM was successfully used to drill micro-sized holes, in which the biggest

was 7.5 μm and the smallest was 30 nm in diameter, on the hollow glass microspheres with diameter of 0.2 mm and thickness of 1 μm. Several kinds of metallic nanofilms were grown by pulsed laser deposition (PLD) method, such as self-assembly Co nanofilms (Fig.3(a)) and Fe/Al alloy nanofilms. The PLD method was also applied to embed Co nanopowders into $BaTiO_3$ nanofilms to form composite nanofilms (Fig.3(b)). The voids in the Co nanofilms were in hexagonal shape with diameter of 20-25 nm.

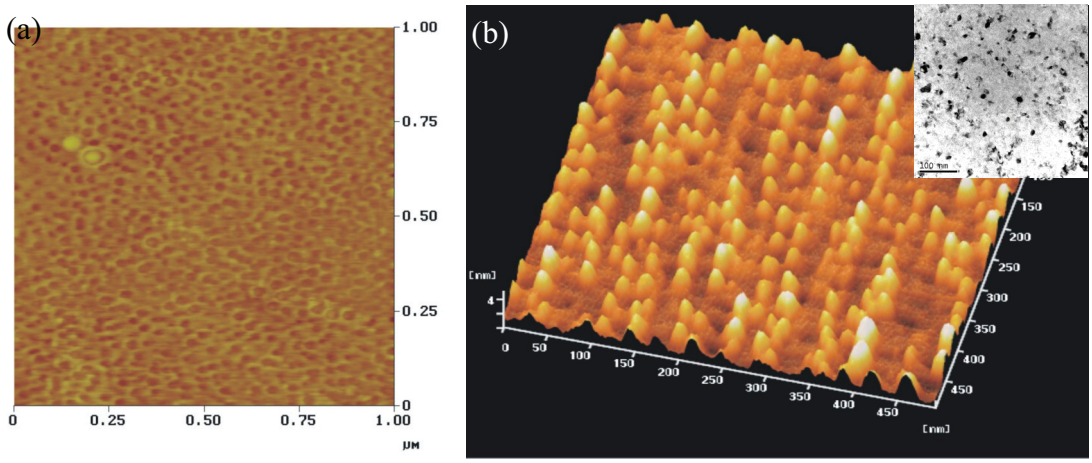

Fig.3 AFM images of (a) self-assembly Co and (b) Co embedded $BaTiO_3$ nanofilms. Inset of (b) shows the TEM image of Co nanopowders with diameter of 15-40 nm in the $BaTiO_3$ matrix, bar=100 nm.

The nanopowders in films can be forced to grow in a definite direction by setting an external electric filed (EEF) through the matrix during deposition. Fig.4(a) and (b) show the effect of an EEF on the growth and shape of Ag nanopowders in $BaTiO_3$ matrix.

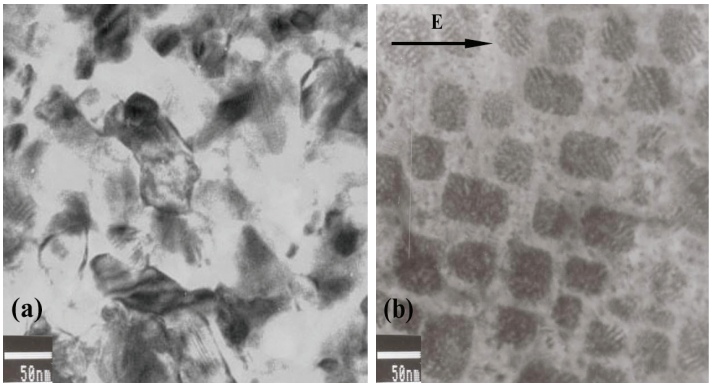

Fig.4 TEM images of Ag embedded $BaTiO_3$ nanofilms: (a) without and (b) with an external electric field of 1000V/cm. The arrow in (b) indicates the direction of the external electric field.

Nanopowders

In 1989, polytetrafluoroethylene powders were efficiently fabricated, of which the morphology was spherical with several to tens of microns in diameter. They were obtained by first irradiating the polytetrafluoroethylene by X-ray or electron beam and then mechanically milling. The yield might be up to a few kilograms per month. However, this method had to be discarded because of environment problem. In 1994, C_{60} and C_{70} cluster materials with purity as high as 99.99% were

successfully synthesized. A production line was built up and was able to produce 1 gram C_{60} powders each day. Resorcinol formaldehyde (RF) and carbonized RF aerogel nanopowders were successfully synthesized. The aerogel nanopowders showed significant capability of absorbing hydrogen, indicating their potential use in hydrogen storage (Fig.5).

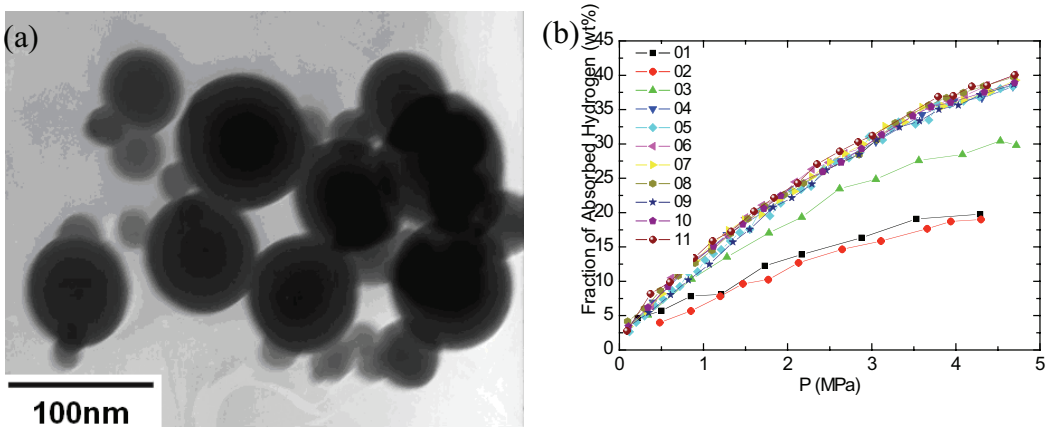

Fig.5 (a) TEM image of carbonized RF aerogel nanopowders, (b) the fraction of hydrogen absorbed by carbonized RF aerogel nanopowders as a function of the hydrogen pressure. The absorption experiments were repeated for eleven times, as shown by different symbols.

In 1993, an electromagnetic-induction-heating-flow-levitation (EHFL) method was devised to produce metal nanopowders [5,6]. In 1997, a set of equipment based of the EHFL method was designed and built to produce nanopowders with diameter over several nanometers. With this equipment, both yield and purity of metal nanopowders were improved highly. In principle, metal wire was first heated by a highly-frequency electromagnetic induction coil so that a metal liquid droplet was formed. The droplet was levitated and heated continuously under its interaction with a magnetic field generated by another reverse electromagnetic induction coil. Atoms at surface of the droplet were evaporated when a high-enough temperature was reached. These evaporated atoms were quickly cooled through their collision with inert gas atoms and formed nanopowders. When inert gas with a special gradient pressure was imposed in the vapor environment, metal atoms and resultant nanopowders would flow along a definite direction with no contact with the reactor wall and finally enter a collector (Fig.6(a)).

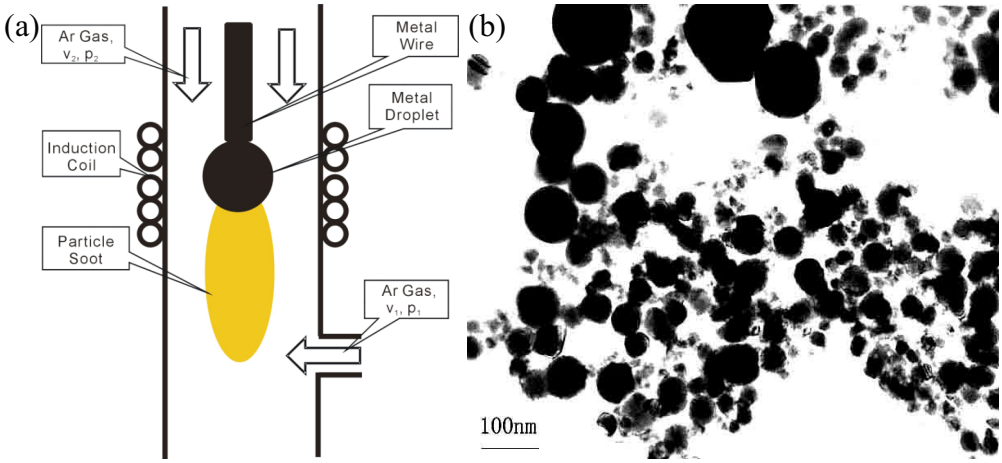

Fig.6 (a) Schematic chart of the EHFL method, (b) TEM image of Cu nanopowders produced by the EHFL equipment.

Using this equipment, metals such as Cu (Fig.6(b)), Ag, Fe, Ni, Al, and Ti and bimetallic nanopowders such as CuAl, NiAl, and TiAl were produced. By compacting these nanopowders in strengh-die under high pressure at room temperature, metal nanocrystalline foils were obtained. The Cu nanocrystalline foils had density 95% of bulk copper, and showed micro hardness 3 - 4 times of that of coarse-grained Cu [7].

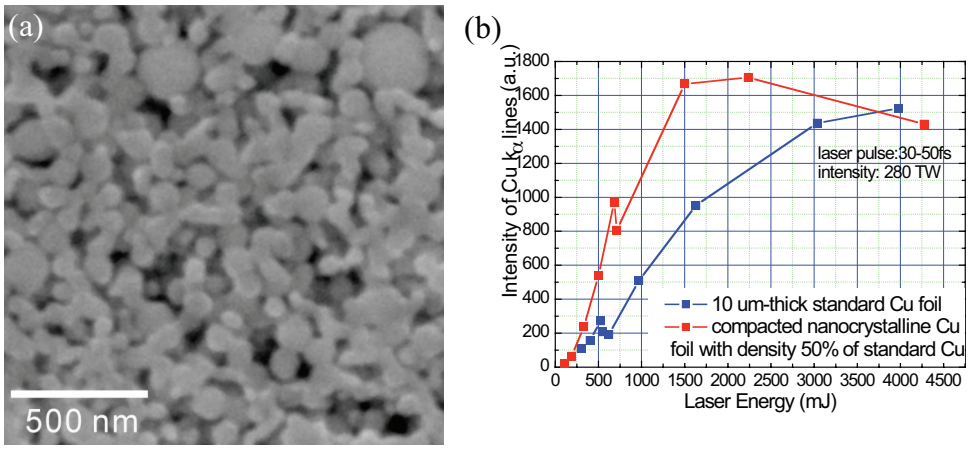

Fig.7 (a) SEM image of nanocrystalline Cu foil with 50% density of standard Cu. (b) Intensity of emitted Cu K_α lines as a function of the incident laser energy when irradiating standard Cu foil and the compacted Cu nanocrystalline foil by ultra fast high power laser.

Interaction of nanocrystalline Cu foil with ultra fast high power laser was investigated. A compacted nanocrystalline Cu foil with 50% density of standard Cu (Fig.7(a)) was irradiated by the SELEX-I laser facility at RCLF, with a pulse width of 30-50 fs and power of 280 TW. The intensity of emitted Cu K_α lines as a function of the incident laser energy is shown in Fig.7(b). For comparison, the result from a 10-μm-thick standard Cu foil is also shown. Obviously, the laser-to-X-ray conversion efficiency in the nanocrystalline Cu is strikingly enhanced relative to that in the standard Cu. The highest enhanced ratio reaches five times at the laser energy of 650 mJ.

Summary

This article introduces some research progress on nanomaterials at RCLF of China by focusing on new results of nanofoams, nanofilms, and nanopowders. These nanostructured materials have been applied to ICF experiments, and further efforts will be made to obtain greater improvement on laser-target interaction performance.

Acknowledgement

All works mentioned were financially supported by the High Technique Foundation and Double-Hundred-Talent Funds of Academy of Engineering Physics in China. The author thanks Dr. L. Zhang, Dr. W.-D. Wu, Dr. C-Y. Wang, Mr. J-S. Luo, Dr. Y-G. Wang, Dr. W. Hong, Dr. J.-J Wei, and Dr. H. Lei for presenting their research works and achievements.

Reference

[1] F-H. Jiang and L.-Q. Zhang, *Atomic Energy Science and Technology* (in Chinese) **33**, 309 (1999).

[2] W.-Y. Jiang, Y. Huang, and H. Xu, *Function Materials* (in Chinese) **27**, 350 (1996).

[3] L. Zhang, Y.-J. Tang, K. Du, et al, *Nuclear Instruments and Methods* A **480**, 242 (2002).

[4] H.-Y. Tu, L. Zhang, K. Du, et al, *Atomic Energy Science and Technology* (in Chinese) **36**, 348 (2002).

[5] H. Lei, Y-J. Tang, J. Li, et al, *Appl. Phys. Lett*. **88**, 083111 (2006).

[6] C-M Li, H Lei, Y-J Tang, et al, *Nanotechnology* **15,** 1866 (2004).

[7] Y.-J. Tang, J.-S. Luo , W. Liu, et al, Proceedings of the International Conference on Nanomaterials (India), **1**, 175, (2005).

Concept of Laser Fusion Power Plant Based on Fast Ignition

T. Norimatsu [1], and Members of Reactor Design Committee

[1] Institute of Laser Engineering, Osaka University, Suita, Osaka 5650871 Japan.
Contact person; norimats@ile.osaka-u.ac.jp

Recent progress on fast ignition (FI) and cooled Yb:YAG ceramic laser enable us to design an IFE power plant with a 1MJ-class, compact laser whose output energy is 1/4 of previous central ignition scheme. Basing on the FI scheme, we conceptually designed a laser fusion power plant driven with cooled-Yb:YAG, ceramic lasers. The cooled Yb-YAG ceramic was newly chosen as the laser material. We found that the heating laser for ignition could be constructed with the cooled Yb:YAG ceramics as well as the compression laser with acceptable electricity-laser conversion efficiencies including the electric power for the cooling system. A new reactor scheme for a liquid wall reactor that has no stagnation point of ablated gas was proposed.

1. Introduction

The fast ignition scheme is very attractive because a high gain can be achieved with smaller lasers that were considered to share major part of the construction cost of a laser fusion power plant. In 2002, our fast ignition experiments with a petawatt (PW) laser in Osaka University demonstrated a heating efficiency of 20 - 30 % at ignition-equivalent laser intensity.[1] This promising result promoted design activity to figure out the final goal for the power plant. After a report of the Roadmap Committee of IFE Forum[2], we organized a Design Committee of Laser Fusion Power Plant 1) to make a reliable scenario for the fast ignition power plant based on the latest knowledge of elemental technologies, 2) to identify the research goal of the elements and 3) to make the critical path clear.

In our previous KOYO design based on central ignition scheme, 4 modular chambers were driven by turns with 4MJ/pulse, 10 Hz lasers to yield 4000-6000MWth fusion energy and 2400MW electric power[3]. The laser was a glass laser (HAP4) driven by diodes. The first wall of the chamber was protected with arrayed SiC composite panels whose surfaces were covered by liquid LiPb films penetrating through the pipe walls. The critical point of this design was poor ability of vacuum pumping by cryogenic effect. When the flows on the SiC pipes were simple laminar flows, the surface temperature near the bottom of the reactor become too high to evacuate ablated metal vapor in the designated time.

In this design work, 1) cooled Yb-YAG ceramic lasers were newly used for compression and heating lasers. 2) The target gain was evaluated using latest simulation codes. 3) Cascade-type, liquid- wall chambers are employed as the modular reactors. 4) The ablation of the first liquid wall and the chamber clearance were discussed basing on new idea of stagnation-free chamber geometry. 5) Scenario for fuel loading in batch process was proposed. In this paper, laser system and chamber issue are discussed focusing on behavior of ablated first wall material.

2. Gain Estimation

The gain performance for fast ignition targets was evaluated by parametric numerical study using 2-D burn simulation code based on 1-fluid 2-temperature Eulerian hydrodynamic code written in 2-D cylindrical coordinates (r-z). The electron thermal conduction, radiation effect, α-particle heating and external fast heating are taken into account. The radiation and the α-particle transports are treated by multi-group flux-limited diffusion model. As the initial core profile, we assumed uniformly-compressed DT spherical plasmas (ρ = 300 g/cc, T = 0.2 keV, α = 2) at the center of the simulation box. With regard to the external fast heating, uniform heating rate was assumed in the cylindrical region (30 μm spot diameter, 1.0 g/cm^2 optical depth) at the core edge for 10 ps. For gain estimation, the coupling efficiencies from the laser to the core plasma were assumed as 5% for implosion and 30% for the core heating. The obtained gain curve is plotted in Fig.1. To achieve the explosive burning and then the high gain (>100), the required compressed core ρR must be larger than 1.6 g/cm^2, and total driver must be higher than 300 kJ.

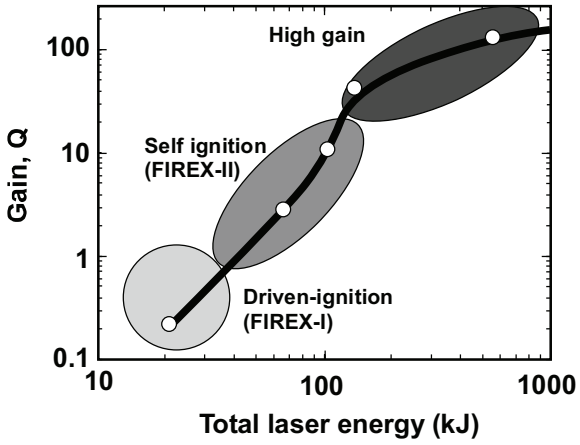

Fig. 1 Estimated gain of fast ignition targets

3. Targets

Targets for a future laser fusion reactor must be designed considering survival of the cryogenic layer during the flight to the reactor center. The environment can be classified into two fields: one is a hot (>1300 K, 0.5 Torr) Xe gas in a dry wall chamber such as Sombrero [4] and the other is a metal vapor such as LiPb of < 0.05 Torr, 900K in the Koyo reactor. In the former case, the thermal radiation and the forced convection heating is the main thermal load on the cryogenic target and, in the latter case, the latent heat of condensation of the metal vapor is the major heat load because almost all of the metal vapor atoms colliding with the surface condense in the first collision due to the very large latent heat of condensation. In both cases, an insulation layer with middle density foam gives a good solution for such heat load [5, 6].

Figure 2 is a baseline target for future laser fusion reactor. This target consists of a heavy LiPb cone whose inner surface is paraboloid and a foam-insulated cryogenic fuel shell. The shell is imploded by a 1.1MJ laser to make a high density core that is directly heated with a 100 kJ heating laser, resulting in a thermonuclear yield of 200 MJ.

Basic specification	
Compression laser	1.1 MJ
Heating laser	70kJ
Gain	165
Fusion yield	200MJ

Fuel shell		
DT(gas) (<0.01mg/cc)	1,500	μm
DT(Solid) (250mg/cc+10mg/cc Foam)	300	μm
Gas barrier (CHO, 1.07g/cc)	2	μm
CH foam insulator (250mg/cc)	150	μm
Outer diameter	1,952	μm
Mas of fuel	2.57mg	
Total Mas of shell	4.45mg	

Cone	
Material	Li17Pb83
Length	11mm
Diameter	5.4 mm
Mas	520 mg

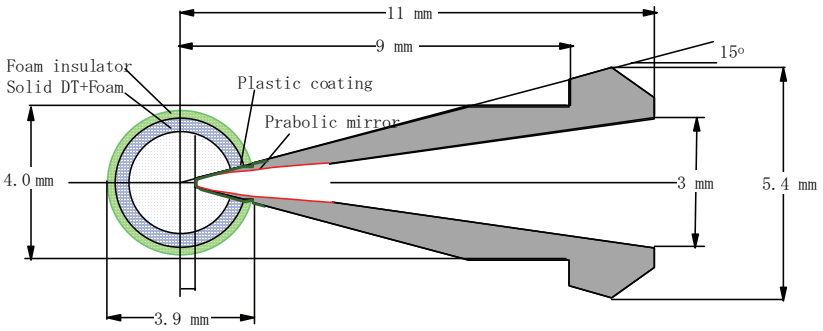

Fig 2 Cross sectional view of fast ignition target for reactor

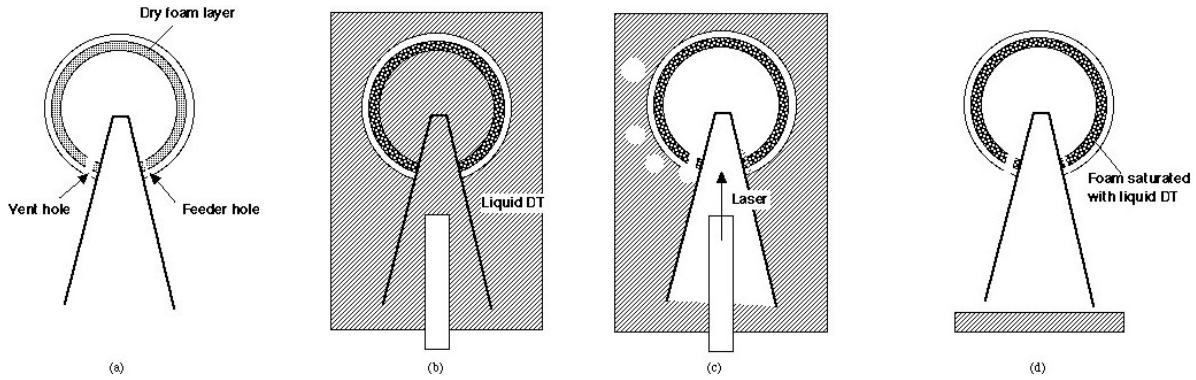

Fig. 3 Proposed fuel loading by batch process

This target is injected into the chamber such that the cone leads the shell. Use of the heavy cone has many merits for reactor use; 1) to stabilize the trajectory against the flow of vapor and drag force in the chamber [7], 2) to work as a heat capacity against the thermal load by condensation of the vapor, 3) to shield the shell against aerosols in vapor, 4) to provide protective material for the first wall of a dry chamber. The parabolic configuration of the inner surface works as a focusing device of the heating laser. In a future power plant, the final optics will be located >30 m from the center to reduce the neutron load. Assuming f = 7, the beam waist at the reactor center is about 300 μm, which is too large to ignite the core. So, some focusing mechanism is necessary in the FI scheme.

Fabrication of such cone seems quite challenging. The hot press method with LiPb is the candidate to make the cone in a batch process. LiPb was chosen because it is the same material as the first wall of the wet reactor and Li in Pb reduces the erosion of the mandrel. Although LiPb is slightly harder than pure Pb, some additional, doping may necessary to improve the ease of handling of the soft cone.

Another issue in mass production of the cone target is fuel loading. Conventional diffusion loading is less attractive because of the large tritium inventory. Injection filling [8] is an ideal method in the viewpoint of the tritium inventory but drilling of the injection hole, precise control of injecting liquid DT must be carried out under cryogenic temperature, which is challenging technique. We propose a new method based on thermal cavitation technique [9] as shown in Fig. 3. This target has two holes with different radii around the cone, larger one is a vent hole and smaller one is a feeder hole. This target is immersed in liquid DT with the cone downward. Liquid DT penetrates into the foam layer through the holes and finally fills the central void in a few seconds (b). Then, laser that is guided with an optical fiber heats the top of the cone. Evaporation of liquid DT takes place in the void and the vapor eliminates the liquid in the void but the foam is still saturated with liquid DT because of the smaller diameter of the cell of foam. Extra vapor blows out through the vent hole (c). Extra liquid in the meniscus no longer exists. To compensate the evaporated liquid from the foam layer, new liquid continuously flows into the foam through the feeder hole. At an appropriate time, the target is pulled out of liquid DT and the laser is turned off (d).

This method enables the foam layer to remain wet without special power control of the laser. The only one required condition is; the radius of foam cell<< the radius of feeder hole < the radius of vent hole << the radius of foam shell, which is easily achieved. Please note that two independent holes are not necessary. A single gap between the cone and shell works as well.

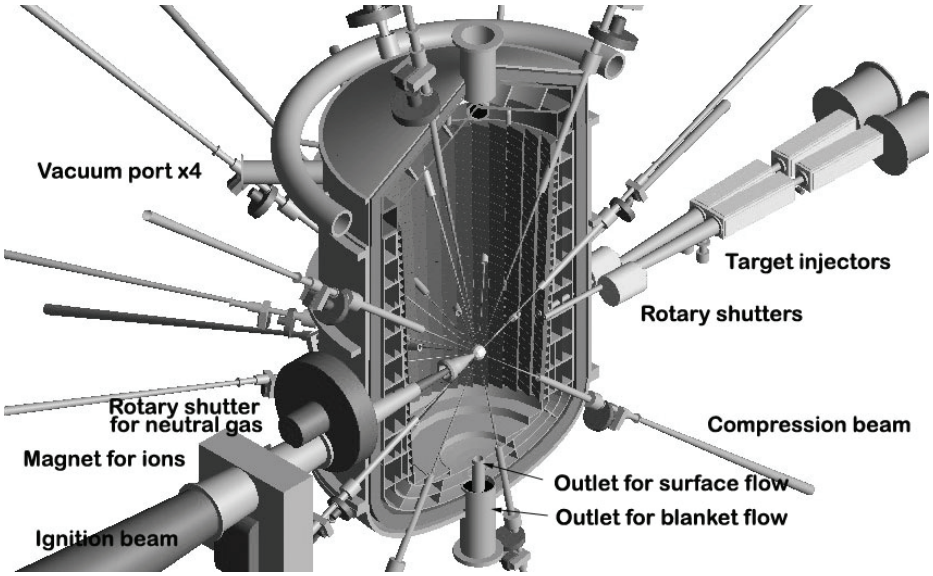

Fig. 4 Cross section of a modular reactor of KOYO-F. The target is emphasized by 150 times for visibility.

4. Chamber

Figure 4 shows a cross section of the modular reactor of KOYO-F. The power plant KOYO-F has 4 modular reactors. Each reactor is operated at 4 Hz by turn. Main features of this design are as follows. 1) the fire position is vertically off-set to simplify the protection scheme of the ceiling. 2) There is no horizontal area on the ceiling to avoid formation of droplets.[10] 3) The first wall is liquid LiPb with cascade flows to obtain fast pumping of evaporated vapor by

cryogenic effect. If the surface flow is a simple laminar flow, the surface temperature becomes too high to obtain cryogenic pump effect when it reaches near the bottom of the chamber. 4) The first panels are tilted by 30 degree to avoid stagnation of evaporated vapor. In the case of KOYO-F, 10kg of LiPb evaporates after a laser shot. If the evaporated vapor collides at the center and loses its momentum, it becomes difficult to obtain high repetition rate. 5) The final optics are protected by compact rotary shutters and buffer gas in the beam duct. 6) Each modular reactor has two injectors that are alternatively operated at 2 Hz. This slow injection rate comes from evacuation of residual gas in the barrel of the gas gun.

The thermal load on the ceiling is close to that of dry wall design. To avoid blistering of the first wall, temperature of the ceiling is kept slightly lower than the other area to form a thin, protective liquid-LiPb membrane. The material of the ceiling must be wetable with LiPb to make continuous membrane. The lifetime of such material due to erosion is a future issue.

Ablation of the liquid Pb was calculated using DECORE (DEsign COde for reactor) that included atomic model, equation of state, phase change, radiation heat transfer and hydrodynamic equations. Influence of Li was ignored for simplification.

After repeating several bounce of the blast wave, residual vapor in the chamber becomes quasi- homogeneous where we can ignore hydrodynamic motion of residual gas. If we assume that fast component uniformly fill the chamber, the pressure in the chamber becomes order of 100 Pa. The heating effect of surface by the blast wave at the first bounce can be ignored in the view point of condensation coefficient because pulse width of blast wave is expanded to an order of 10 ms. So, residual gas in the chamber will be continuously evacuated to the designated pressure of 5-10 Pa before the next laser shot.[11]

When we look into a horizontal cross section of the chamber, ablated vapor from the bottom reaches on the ceiling with some interaction with vapors from the side wall. If we assume that ablated vapor from the bottom uniformly condenses on the ceiling, the thickness of condensed LiPb layer is 2.5 μm/shot that is larger than ablation rate. Of course this is too preliminary to discuss the formation of protection layer, we believe we can form the protection layer by enhancing condensation of residual vapor, especially lithium, in the chamber by keeping the surface temperature less than the other area in the chamber.

Another critical issue of this concept is protection of beam ports ejecting from the liquid surface. The top of the port is directly exposed to the radiation from the plasma. Our current solution is to use a porous plate through which liquid LiPb penetrate from inside. The temperature of the port is also kept colder than other area to enhance the condensation. If we assume the maintenance period of two years, the possibility for direct exposure must be less than $1/10^4$. More detailed research based on experiment is necessary to discuss the reliability of liquid wall scheme.

5. Summary

We have examined the design windows and the issues of the fast ignition laser fusion power plants. ~1200 MWe modular power plants driven at ~16 Hz The basic specification is summarized in TABLE II. For laser driver we have considered the DPSSL design using the

Yb:YAG ceramic operating at low temperature (~200K). We have proposed the free fall cascade liquid chamber for cooling surface quickly enough to several Hz pulses operation by short flow path. The chamber ceiling and laser beam port are protected from the thermal load by keeping the surface colder to enhance condensation of LiPb vapor.

TABLE II: BASIC DESIGN PARAMETERS FOR THE POWER PLANT KOYO-F

Net electric output	1283 MWe (320 MWe x 4)
Electric output from one module	320 MWe
Target gain	167
Fusion Yield	200 MJ
Laser energy / Beam number	1.2 MJ (Compression=1.1MJ/32beams, Heating=100kJ 1beam)
Laser material / Rep-rate	Cooled Yb:YAG ceramics at 150 - 220K /16 Hz
Chamber structure / Rep-rate at module	Cascade-type, free-fall liquid LiPb wall/4 Hz
Fusion power from a module	800 MWth
Blanket gain	1.2 (design goal)
Total thermal output from a module	916 MWth
Total thermal output from a plant	3664 MWth (916 MWth x 4)
Heat-electricity conversion efficiency	41.5% (LiPb Temperature 500 ^{o}C)
Gross electric output	1519 MWe
Laser efficiencies	13.1% (compression), 5.4% (heating), Total 11.8% (including cooling power)
Recirculating power for laser	164 MWe (1.2 MJ x 16 Hz / 0.118)
Net electric output/efficiency	1283 MWe (1519 MWe - 164 MWe - 72 MWe Aux.)/32.7%

TABLE III: MEMBERS OF REACTOR DESIGN COMMITTEE.

Steering board Y. Hirooka (NIFS.), F. Kan (Hamamatsu Photonics), M. Kikuchi (JAEA), T. Konishi (Kyoto Univ.), A. Koyama (Kyoto Univ.), K. Mori (Kawasaki Plant), T. Muroga (NIFS), M. Nishikawa(Kyushu Univ.), M. Nishikawa (Osaka Univ.), Y. Ogawa (Tokyo Univ.), K. Okano (CRIEPI.), M. Onozuka (Mitsubishi Heavy Ind.), Y. Owadano (AIST.), A. Sagara (NIFS.) Y. Suzuki (Laser Front Technol.), K. Tanaka (Nisshin Co.), N. Tanaka (Mitsubishi Heavy Ind.), K. Ueda (Univ. Electro-com.), Y. Ueda (Osaka Univ.), T. Yamanaka (Fukui Univ.), H. Azechi (ILE), N. Miyanaga (ILE), K. A. Tanaka (ILE)
Core working group H. Azechi (ILE), Y. Nakao (Kyushu Univ.), H. Sakagami (Hyogo Unv.), H. Shiraga (ILE), R. Kodama (ILE), H., Nagatomo(ILE), T. Johzaki (ILE)
Laser working group N. Miyanaga (ILE), Y. Suzuki (Laser Front Technol.),K. Ueda (Univ. Elector-Com.), N. Tuchiya (Nishin Co.) Y. Oowadano (AIST), T. Jitsuno (ILE), M. Nakatsuka (ILE),H. Fujita (ILE), K. Yoshida (Osaka Inst. Technol.), J. Kawanaka (ILE), H. Nakano (Kinki Univ.), Y. Fujimoto (ILE), H. Kubomura (HP), T. Kawashima (HP), S. Matsuoka(HP), T. Ikegawa(HP), K. Tusbakimoto (ILE), J. Nishimae (Mitsubishi Elec.), H. Furukawa (ILT)
Target working group T. Norimatsu (ILE), M. Nishikawa (Kyushu Univ.), Konishi (Kyoto Univ.), T. Endo (Hiroshima Univ.), H. Yoshida (Gifu Univ.), N. Mituo (ILE)
System working group Y. Kozaki (ILE), Y. Soman (Mitsubishi Heavy Ind.), K. Okano (CRIEPI), H. Furukawa (ILT), Y. Sakawa (Nagoya Univ.), A. Sagara (NIFS), T. Norimatsu (ILE)
AIST; National Institute of Advanced Industrial Science and Technology, CRIEPI; Central Research Institute of Electric Power Industry HP; Hamamatsu Photonics, ILE; Institute of Laser Engineering, Osaka University, ILT; Institute for Laser Technology, Osaka JAEA; Japan Atomic Energy Agency, NIFS; National Institute for Fusion Science

6. Acknowledgement,

This work was partly supported by the JSPS-CAS Core-University Program in the field of "Plasma and Nuclear Fusion".

References

[1] KODAMA, R., et al., “Fast Heating Scalable to Laser Fusion Ignition” *Nature*, 418, 6901 (2002).
[2] KOZAKI, Y., “Power Plant Concepts and Chamber Issues for Fast Ignition Direct Drive Targets”, *Fusion Sci. Technol.,* **49**, 542 (2006).
[3] NAKAI, S., et al., *Sixteenth IAEA Fusion Energy Conference*, Montreal, Canada, 7-11 October, 1996, IAEA-CN-64/G1-3/GP-17
[4] W. R. Meier, “Osiris and Sombrero Inertial fusion power plant designs - Summary, conclusions and recommendations,” Fusion Eng. Des., 25 145 (1994).
[5] T. Norimatsu, et al., "Influence of gases on direct-drive cryogenic targets in laser fusion reactor with wet wall," Fusion Eng. Design. 65, 393 (2003),
[6] T. Norimatsu, et al., Proceeding of Inertial Fusion Science and Application 2001, Sept. 10-14, 2001 Kyoto, Elsevior (France) 2002, p752 "Foam insulated direct-drive cryogenic target."
[7] T. Norimatsu, et al., "Update for the drag force on an injected pellet and target fabrication for Inertial fusion," Fusion Sci. Technol. 43, 339 (2003).
[8] M. J. Monsler, Y. A. Merkul'ev and T. Norimatsu, pp. 151"Energy from Inertial Fusion", IAEA, Vienna (1995) ISBN 92-0-100794-9, "Target fabrication and positioning."
[9] T. Norimatsu et al., “Development of FI Targets for FIREX and Issue on Mass Production and Delivering of FI Target with Cone for Power Plant Reactor,” Presented at FIHEP2004, April 26, 2004, Kyoto Japan.
[10] SHIN, S., ABDELALL, F., JURIC, D., ADBDEL-KHALIK, S. I., YODA, M., SADOWSKI, D., and THE ARIES TEAM, “Fluid Dynamic Aspects of the Porous Wetted Wall Protection Scheme for Inertial Fusion Energy Reactors”, *Fusion Sci. Technol.,* **43**, 366, (2003).
[11] KOZAKI, Y., YAMAMOTO, K., FURUKAWA, H, and AWATA, N., “Vapor Evacuation and Issues of Liquid Wall Chamber”, *Ann. Prog. Rpt. ILE Osaka*, 149 (2000).

Impact Fast Ignition

M. Murakami, H. Nagatomo, T. Sakaiya, S. Fujioka, H. Saito, H. Shiraga, M. Nakai, K. Shigemori, H. Azechi, M. Karasik, J. Gardner, J. Bates, D. Colombant, J. Weaver, A. Schmitt, A. Velikovich, Y. Aglitskiy, J. Sethian, and S. Obenshain

Institute of Laser Engineering, Osaka University, 565-0871 Osaka, Japan
Naval Research Laboratory, Washington D. C., 20375, USA

Introduction

Recently, we have proposed a totally new ignition scheme – impact fast ignition (IFI) [1,2]. Figure 1 shows the initial target structure of the impact ignition overlapped with the compressed fuel image at maximum compression. The target is composed of two parts: a spherical pellet made of DT shell coated with an ablator and a hollow conical target, which is stuck to the spherical pellet. The conical component has a fragmental spherical shell (impact shell) also made of DT and an ablator. The key idea is to accelerate the impact shell to collide against the main fuel. On the collision, shock waves generated at the contact surface transmit in two opposite directions heating the fuels to produce an igniting hot spot. In this case, the impact shell itself becomes the ignitor by

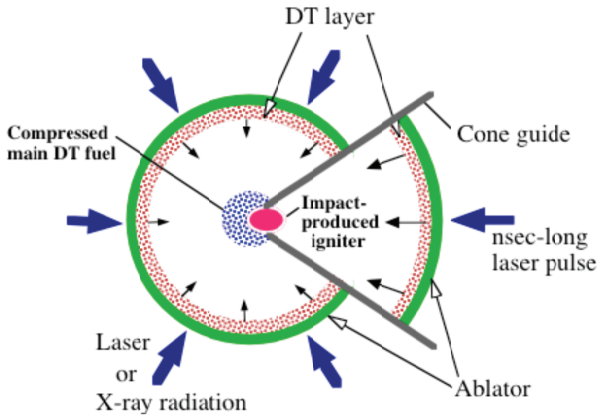

Fig. 1 Initial target structure of the impact fast ignition (IFI) target overlapped with the compressed fuel image at maximum compression.

directly converting its kinetic energy into the thermal energy rather than to boost the main fuel heating as in the particle (electrons or ions) -driven fast ignition. It is then necessary for a high coupling efficiency from the driver energy to the thermal energy of the ignitor that the impact shell is accelerated ablatively.

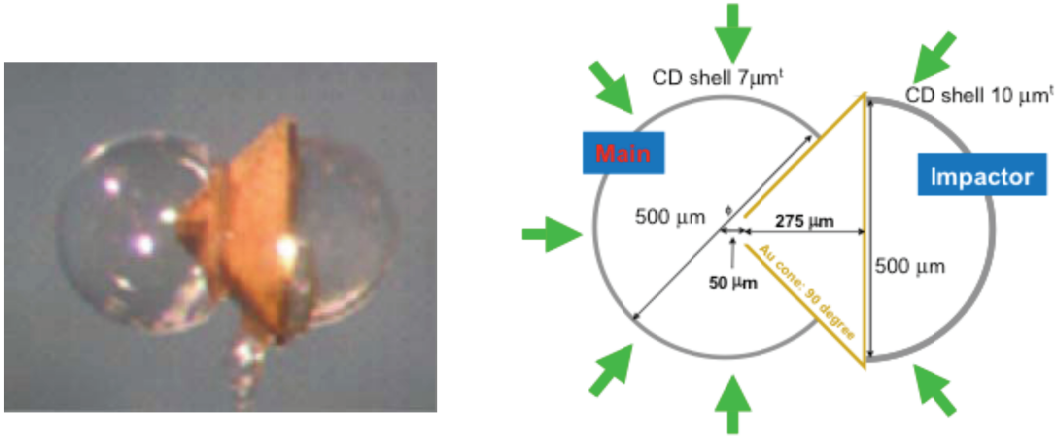

(a) **(b)**

Fig. 2 (a)Picture of the integrated target (b) Schematic view of the target

First Experiments with Integrated Targets and Neutron Yields

Besides the super-high velocity experiments, we have recently done experiments with an integrated target, which is composed of two CD semispherical targets bonded by the gold cone as can be seen in Fig. 2. The gold cone has an open hole of 50 μm in diameter at the tip. In the experiments, 3 beams for 1.0 kJ and 9 beams for 3.2 kJ of Gekko XII laser system with 0.35 μm of wavelength, 1.3 ns (FWHM) of pulse length in Gaussian pulses were used to irradiate the impactor and the main fuel hemispheres respectively. Figure 3 shows the timing relation between the implosion laser and the impactor laser (a) and the resultant neutron yield as a function of the laser timing. For example, the laser timing of –1 ns means that the impactor laser beams are irradiated 1 ns prior to the implosion lasers. As can be seen in Fig. 3, there is an optimum laser timing to maximize the neutron yield to achieve the neutron yield of $2\text{x}10^6$. The neutrons are produced mainly in the impactor CD shell, which follows and supports the very original idea of the impact fast ignition scheme. Further more, Fig. 3(b) shows that the laser timing is an crucial parameter in designing the IFI target.

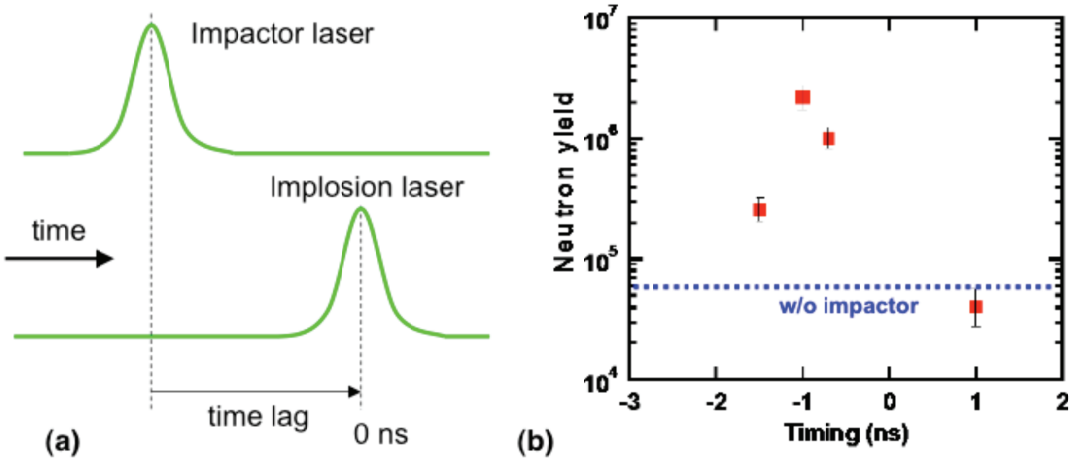

Fig. 3 (a) Definition of pulse timing (b)Neutron yields with integrated IFI target

Acknowledgement, This work was partly supported by the JSPS-CAS Core-University Program in the field of "Plasma and Nuclear Fusion".

References

[1] M. Murakami and H. Nagatomo, Nucl. Instrum. Meth. Phys. Res. A **544** (2005) 67.

[2] M. Murakami *et al.*, Nucl. Fusion **46** (2006) 99.

Synthesis of Nanomaterials and Their Applications in Biosensors and Bioelectronics

Xinghua Xia*, Yanyan Song, Wei Chen, Ya Ding, Wenzhi Jia

Key Laboratory of Analytical Chemistry for Life Science, School of Chemistry and Chemical Engineering, Nanjing University, Nanjing 210093, China.

Nanomaterials are promising for the construction of functional biointerfaces for bioelectronic devices and biosensors. Recent reports have shown that nanomaterials could be ideal electron mediators or ideal nano-interfaces for biomolecules due to their unique properties. In addition, they could provide appropriate microenvironments to retain the bioactivity of the immobilized biomolecules. We are recently focusing on the construction of nanostructured materials-based functional biointerfaces for electrocatalysis and direct electron transfer of model biomolecules such as hydrogen peroxide [1,3,11], glucose[2,6,8,11], glucose oxidase and heme protein[7,12], etc. The nanostructured materials including 2D films of Prussian blue, silica and others and 3D macroporous structures of noble metals of gold, platinum and hybrid composites have been designed and successfully synthesized using novel galvanic displacement reactions [9], electrokinetic approach [3,5,10,14] and other novel methods. Systematical studies on the thermodynamics and kinetics of electrocatalysis and the assembly of model biomolecules on the functional biointerfaces have been carried out in our group with the help of scanning electrochemical microscopic, electrochemical and in situ spectroscopic techniques. For better understanding the performance of biosensors, the influence of interfacial electric field on the orientation, bioactivity and electron communication of the biomolecules at electrode surfaces have been systematically studied [12]. In addition, we are using the biomolecules-interface hybrid systems as building blocks to fabricate a series of highly sensitive and selective biosensing devices [4,13,15]. Of all these investigations, new concepts for highly sensitive and selective glucose detection based on fast depletion of interfering electroactive species in the diffusion layer of a substrate electrode or shortened detection distance (diffusion-layer-distance gap system) were developed. This concept has been applied to fabrication of microbiosensors.

References:

[1] D. Zhang, K. Wang, D.C. Sun, X.H. Xia, *Chem. Mater.* **2003**, *15*, 4163.

[2] D. Zhang, K. Zhang, Y.L. Yao, X.H. Xia, *Langmuir* **2004**, *20*, 7303.

[3] J.H. Yuan, F.Y. He, D.C. Sun, X.H. Xia, *Chem. Mater.* **2004**,*16*, 1841.

[4] K. Wang, D. Zhang, T. Zhou, X.H. Xia, *Chem. Eur. J.*, **2005**, *11*, 1341.

[5] W. Chen, X.H. Xia, *Anal. Chem.*, **2005**, 77, 8102.

[6] J.H. Yuan, K. Wang, X.H. Xia, *Adv. Func. Mater.* **2005**, *15*, 803.

[7] C.H. Wang, C. Yang, Y.Y. Song, W. Gao, X.H. Xia, *Adv. Func. Mater.* **2005**, *15*, 1267.

[8] Y.Y. Song, D. Zhang, X.H. Xia, *Chem. Eur. J.* **2005**, *11*, 2177.

[9] Y.Y. Song, K. Zhang X.H. Xia, *Appl. Phys. Lett.*, **2006**, 88 (5), 053112.

[10] W. Chen, X.H. Xia, *ChemPhysChem*, **2007**, 8, 1009.

[11] J. Li, J.D. Qiu, J.J. Xu, H.Y. Chen, X.H. Xia, *Adv. Funct. Mater.*, **2007**, 2007, 17: 1574.

[12] Y.Y. Son, C. Yang, X.H. Xia, *Adv. Funct. Mater.*, **2007**, 2007, 2377.

[13] W.Z. Jia, K. Wang, Y.L. Hu,Y.Y. Song, X.H. Xia, *Electrochem. Commun.* **2007,** 9, 1553.

[14] W. Chen, X.H. Xia, *Adv. Funct. Mater.*, **2007**, 17, 2943.

[15] Y. Ding, X.H. Xia, H.S. Zhai, *Chem. Eur. J.*, **2007**, 13, 4197

Recent Study of Target Injection and Tracking at Gifu University

H. Yoshida

(Faculty of Engineering, Gifu University, 1-1 Yanagido, Gifu, 501-1193, Japan)

Introduction

In an IFE power plant, fusion targets have to be injected into the focal area of driver beams in a reactor. For fast ignition, a cone target is provided within a sabot that protects the target from thermal radiation in the injector. The target is accelerated at the acceleration of <500G with the sabot. The target must be spun for accurate injection and minimization of tumbling. Before injection to the reactor, the target is separated from the sabot. A coil gun has been designed and tested for the target injection and tracking at Gifu University.

Target Injection

Fig.1 shows the coil gun which is composed from three kinds of coils: acceleration ones, rotating field ones, deceleration ones. The acceleration ones are energized by capacitors in three phase fashion with a certain time sequence to generate a traveling magnetic field. Propelling force simultaneously acts on the sabot by the interaction between the traveling magnetic field and the induced currents

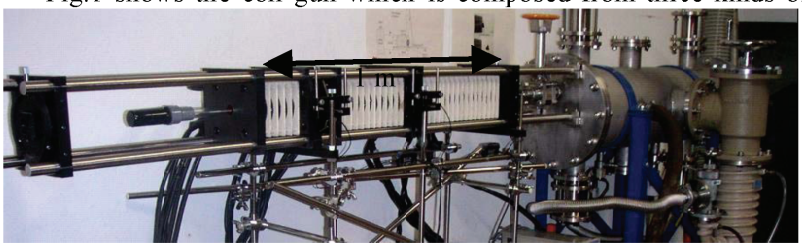

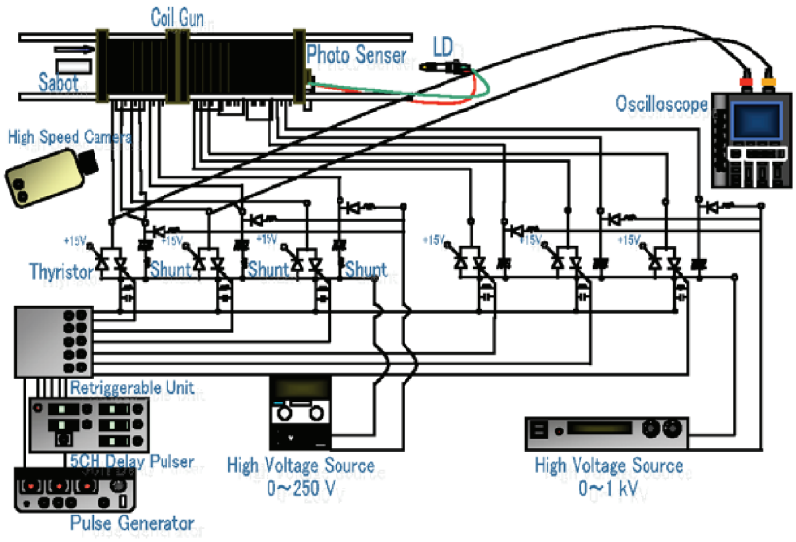

(b)Electrical setup of first and second acceleration coils.

Fig.1 Coil gun system.

in the sabot. A sabot (1-mm-thick aluminum cylinder, 8.86 grams, outer diameter 15 mm, and 75 mm long) can be accelerated at certain acceleration up to 580G by tuning of each coil currents timing. The rotating field coils generate a rotating electromagnetic field which spins the sabot to decrease tumbling of it. For sabot removal, the deceleration coils generate the backward traveling electromagnetic wave which causes negative force on the sabot. The mechanically accelerated target with sabot was sent into the sabot remover. Fig. 2(a) shows a target (6.0mmϕ, 0.2g), a target container, and an aluminum cylinder (15mmϕ×30mm) used as the sabot. An optical fiber sensor was used for synchronizing the sabot arriving timing and generation of deceleration electromagnetic wave. The target and the sabot were monitored by the high-speed camera (KODAK, EKTAPRO 4540) with time resolution of 9000fps. As shown in Fig. 2(b), the target is successfully released from the sabot.

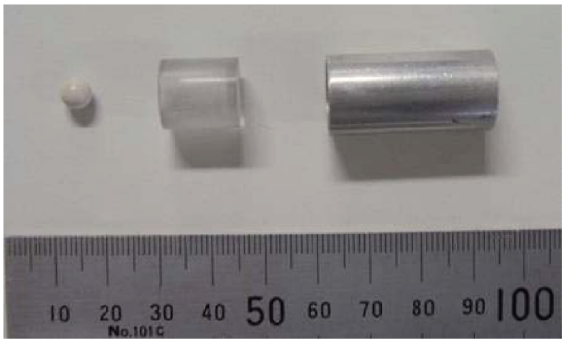

(a) a target, a container, and a sabot

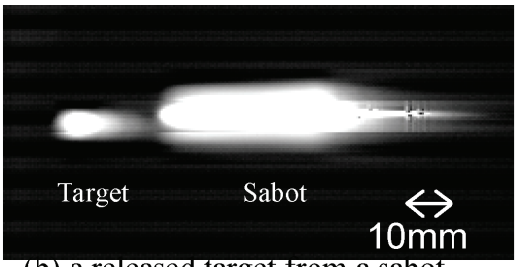

(b) a released target from a sabot
v=30m/s, 9000 fps,
KODAK, EKTAPRO 4540

Fig. 2 Sabot removal by deceleration of a sabot.

Target Tracking

The amplifier-SBS mirror apparatus was tested for a beam steering method. The probe laser beam was provided by a Q-switched Nd:YAG oscillator (τ=6ns, E<50mJ). The apparatus; an amplifier (G = 1~20), a converging lens, and the SBS cell (FC-72) were arranged in a series. The reflected and/or scattered probe beam from target was amplified and was converged into the SBS cell. An HR mirror was used for a target in this experiment. The achieved reflectivity of the SBS cell was ~30%. As shown in Fig.3, the probe beam reflected from the SBS cell was amplified again at energy of 500 mJ and was back-propagated to the target. Target configuration and surface condition are key parameters in this experiment.

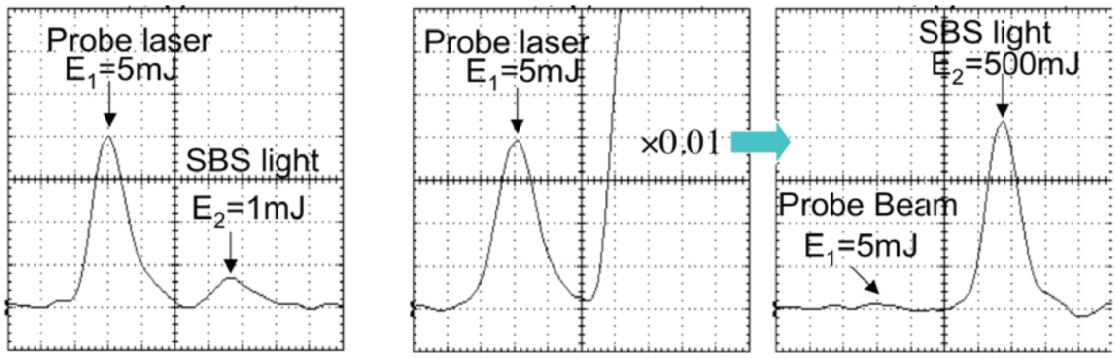

(a) no amplification (b) amplification (G = 20)

Fig. 3 Amplification of the reflected and/or scattered probe laser beam by the amplifier-SBS mirror apparatus.

References

[1] T. Norimatsu, D. Harding, R. Stephens, A. Nikroo, R. Petzoldt, H. Yoshida, K. Nagai, Y. Izawa, Fus. Sci. Tech., **2006**, *49*, 483.

Acknowledgement, This work was partly supported by the JSPS-CAS Core-University Program in the field of "Plasma and Nuclear Fusion".

Magnetic and Electrochemical Properties of an Array of Novel TCNQ Lanthanide Complexes

G.M. Li,[a]* J.W. Zhang,[a] P.F. Yan,[a] G.F. Hou,[a] J.S. Gao,[a] M. Suda,[b] Y. Einaga[b]*

([a]School of Chemistry and Materials Science, Heilongjiang University; No. 74, Xuefu Road, Nangang District, Harbin 150080, China, E-mail: gmli@hlju.edu.cn; [b]Department of Chemistry, Faculty of Science and Technology, Keio University, 3-14-1 Hiyoshi, Yokohama, 223-8522, Japan)

Introduction

Although molecular magnetic materials based on 3d metals and TCNE or TCNQ are quite common, analogous 4f compounds are relatively rare. Recent work by Miller and co-workers have provided the first example in which 4f elements coordinated to $TCNE^{\cdot-}$ yield products that undergo spontaneous magnetization after thermal annealing. Unfortunately, no structural information is yet available for these phases.[1] A notable example is the recent reported compound $\{[CuL]_2Gd(TCNQ)_2\}\cdot TCNQ\cdot CH_3OH\cdot 2CH_3CN$ (L = N, N'-propylenebis (3-methoxysalicylideneiminato)) containing three different types of spin carriers (3d–4f–organic radical).[2] The magnetic properties of this mixed salt are indicative of ferromagnetic coupling between Cu^{II} and Gd^{III} ions with no contribution from the TCNQ radicals, presumable due to the presence of $[TCNQ]_2^{2-}$ dimers. Another worth mentioning example is the only lanthanide TCNQ compound , $\{[Gd_2(TCNQ)_5(H_2O)_9][Gd(TCNQ)_4(H_2O)_3]\}\cdot 4H_2O$.[3] Magnetic data of the compound indicate that some of the magnetic interaction are antiferromagnetic, a situation that leads to define the material as ferrimagnets. Herein, an array of TCNQ lanthanide complexes are prepared and structurally characterized. The magnetic and electrochemical properties are examined.

Description of the Structures

The X-ray crystallography analyses revealed that **1** & **2**, **3-5**, **6** & **7** and **8** & **9** are isomorphous, respectively. Complexes **1-7** are dinuclear compounds, while **8** & **9** are mononuclear compounds. The cationic structure of $[Gd_2(TCNQ)_4(H_2O)_{10}][(TCNQ)_2]\cdot 3H_2O$ (**6**) consists of a dimeric $[Gd_2TCNQ_2]$ unit (Fig. 1). The two Gd(III) ions are bridged by two

$TCNQ^-$ ligands to generate a slightly distorted parallelogram with a Gd(III)···Gd(III) distance of 8.394 Å and the interior angles of 71° and 116°. The eight-coordinate Gd(III) ions are surrounded by three N atoms from three $TCNQ^-$ ligands and five water molecules. The Er(III) ion in $[Er(TCNQ)_2(H_2O)_6][(TCNQ)_{0.5}(TCNQ)_{0.5}]\cdot H_2O\cdot 2MeOH$ (**8**) is coordinated to two $TCNQ^-$ radicals and six water molecules (Fig. 2). Er(III)···Er(III) distance is 8.111Å in crystal packing structure of **8**.

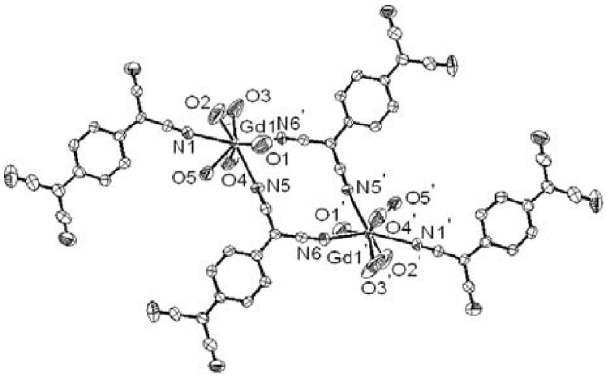

Fig. 1 Cationic structure of compound **6**

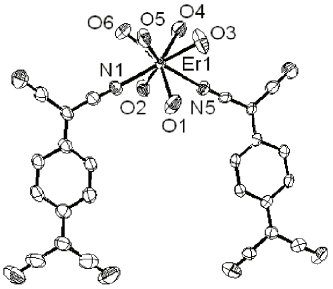

Fig. 2 Cationic structure of compound **8**

Magnetic properties

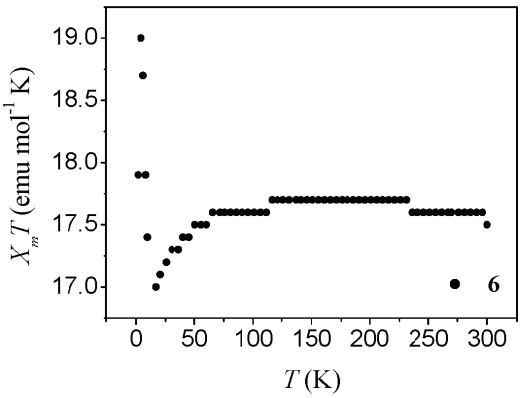

Fig. 3 Plots of $\chi_m T$ vs T for **6**

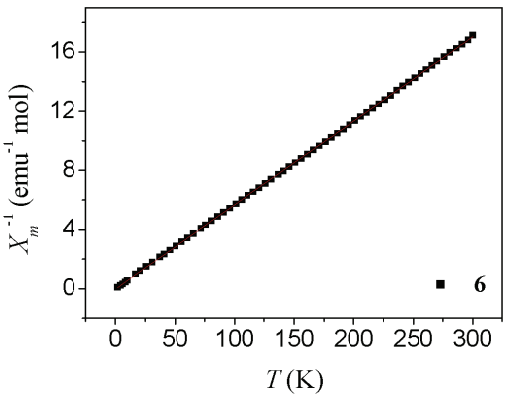

Fig. 4 Plots of χ_m^{-1} vs T for **6**

A variable-temperature magnetic study on $[Gd_2(TCNQ)_4(H_2O)_{10}][(TCNQ)_2]\cdot 3H_2O$ (**6**) was carried out over the temperature range 2-300 K at 500 Oe. The variations of the inverse of the magnetic susceptibility, χ_m^{-1} and $\chi_m T$ of **6** are shown in Fig. 3 and 4. The value of $\chi_m T$ at 300 K for **6** is 17.50 emu·mol^{-1}·K and is in good agreement for two isolated Gd(III) (S = 7/2,

$\chi_m T$ = 7.88 emu·mol^{-1}·K) and four TCNQ$^{\cdot-}$ (S = 1/2, $\chi_m T$ = 0.375 emu·mol^{-1}·K), i.e. 17.26 emu·mol^{-1}·K. The thermal population of χ_m^{-1} obeys Curie-Weiss law, $\chi_m^{-1} = C/(T - \theta)$, over the whole temperature range with Weiss constant, θ = 0.448 K. The magnetic data of **6** indicate a weak ferromagnetic interaction between Gd(III) ions and TCNQ$^{\cdot-}$.

Electrochemical Properties

Cyclic voltammograms of complexes **1-9** (Fig. 5) a reversible one-electron oxidation and one reversible one-electron reduction have been revealed for neutral complexes **1-4**. A reversible one-electron oxidation and one quasi-reversible one-electron reduction have been revealed for neutral complexes **5-8**. However, a reversible one-oxidation has been observed for neutral complex **9**.

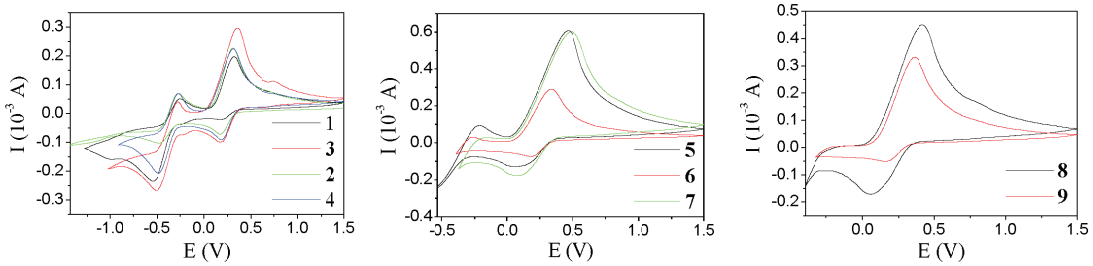

Fig. 5 Cyclic voltammograms of complexes **1-9** in acetonitrile, 0.1 M TBA^{+}PF$_6^{-}$, on glassy carbon electrode versus Ag/AgCl, scan rate 100 mVs^{-1}, potential range from -1.5 V to 1.5 V. TBA = tetrabutylammonium.

References

[1] J. W. Raebiger and J. S. Miller. *Inorg. Chem.* **2002,** *41,* 3308.

[2] A. M. Madalan, H. W. Roesky, M. Andruh, M. Noltemeyer and N. Stanica. *Chem. Commun.*, **2002,** 1638.

[3] H. Zhao, M. J. Bazile, Jr., J. R. GalánMascarós and K. R. Dunbar. *Angew. Chem. Int. Ed.* **2003,** *42,* 1015.

Study of Fuel Layering Processes on the Foam Cryogenic Target for the FIREX Project

A. Iwamoto[1], T. Fujimura[2], M. Nakai[2], T. Norimatsu[2], K. Nagai[2], R. Maekawa[2], T. Mito[2], H. Sakagami[1]

1)National Institute for Fusion Science, 322-6 Oroshi, Toki, Gifu 509-5292, Japan, E-mail: iwamoto.akifumi@lhd.nifs.ac.jp;

2)Institute of Laser Emgineering, Osaka University, 2-6 Yamada-oka, Suita, Osaka 565-0871, Japan

Introduction

The cryogenic target for the Fast Ignition Realization EXperiment (FIREX) project is developed by collaboration between the Institute of Laser Engineering (ILE), Osaka University and the National Institute for Fusion Science (NIFS). The target, called the foam target, has a unique appearance (see Fig.1). The foam is low density plastic, which covers inner surface of the shell as a supporting material of the fuel. The conical laser guide for guiding the heating laser to the core plasma is partially inserted into the shell. To directly supply the fuel, the gas or liquid feeder with 30/10 μm outer/inner tip diameters is connected to the shell. Liquid fuel is fed into the shell though the feeder and is soaked up by the foam material under capillarity. Finally, the fuel is solidified, and an ideal cryogenic target would be foamed.

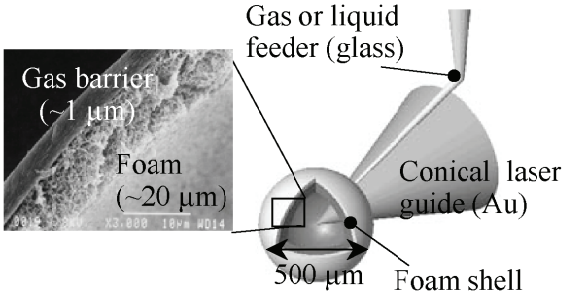

Fig. 1. Foam target for FIREX-I.

Issues for the target development are fabrication of the foam shell, assembling the target, and fuel layering technique. To date, its assembling method had been proved, [1] and an apparatus for cool-down tests have been developed. [2,3] A new fabrication process for the foam shell with a small diameter has been developed at ILE. In the case of the foam cryogenic target, difficulty of the fuel layering is that conventional methods [4,5] may not be applied. Therefore, a suitable layering process for the foam target is being studied. In this paper, a preliminary result of cool-down test using a dummy foam target is described.

Dummy foam target

For preliminary cool-down tests, a dummy foam target was fabricated as shown in Fig. 2. The foam shell is ~800 μm in diameter and ~60 μm in thickness, which was supplied by General Atomics (GA). The shell surface was coated with a parylene membrane (some μm thickness) as gas barrier. The density of the foam material is ~100 mg/cm^3. The shell size is larger than that for FIREX-I (500 μm). However, the property of the foam shell as a supporting material of the fuel can be examined. The laser guide is partially inserted into the shell. The inner tip diameter of the glass feeder is ~20 μm. Its assembling method is the same as that for a typical foam target.

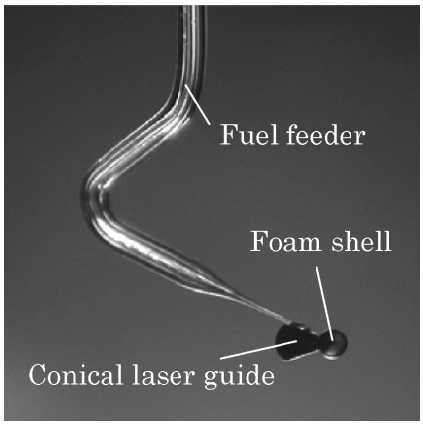

Fig. 2. Dummy foam target.

Demonstration of fuel layering

The target was contained in a target can (see Fig. 3) which was connected to a 4 K GM cryocooler. Exchanged gaseous He (GHe) was filled in the can. The detail of the apparatus is described in reference [2]. Figures 4(a)-(d) show the liquefaction and the solidification sequence in the foam shell. First, the target was cooled down to 13 K. Then, gaseous H_2 (GH_2) was supplied into the foam shell, and liquefaction was started at the pressure of ~8.5 kPa. Liquid quantity was adjustable by controlling both the GH_2 pressure and the exchange GHe temperature. After the foam layer was immersed with an adequate amount of Liquid H_2 (LH_2) (see Fig. 4(b)), the temperature was lowered. At 12.4 K, phase transition to solid was observed. In the case of the foam shell method, solidification did not make the fuel layer opaque. However, the crystallization of the SH_2 appears not to be uniform and some defects are observed (see Fig. 4(c)). Finally, the

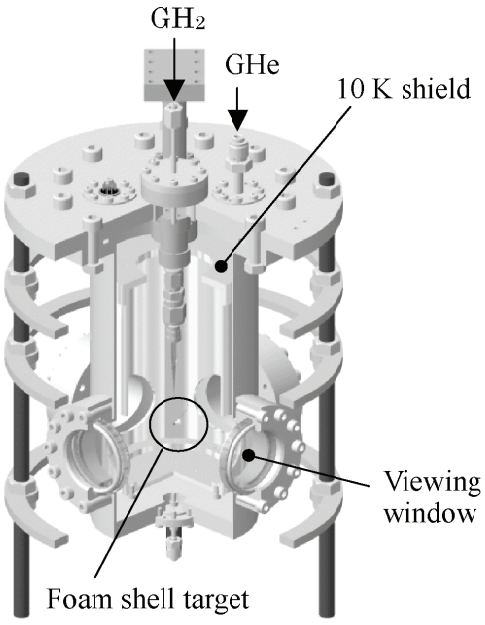

Fig. 3. Target can.

temperature was lowered to 11.8 K in fifteen minutes, and the solid layer might ameliorate (see Fig. 4(d)) because the solid layer looks like the liquid layer of Fig. 4(b).

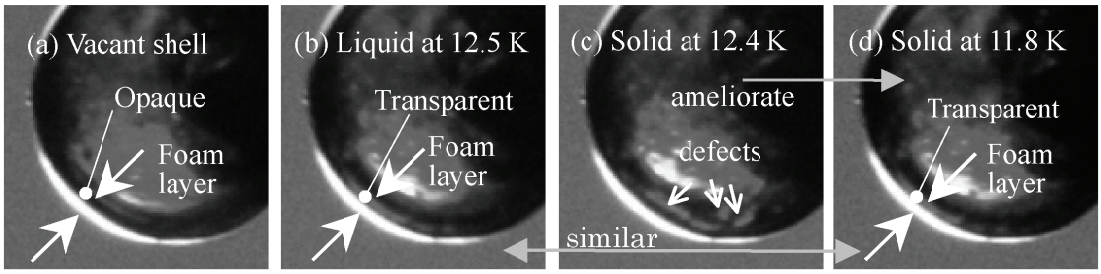

Figs. 4(a)-(d). Sequence of H_2 liquefaction and solidification.

Summary

Fuel layering in the dummy foam shell target was preliminary demonstrated. The LH_2 appears to be uniformly filled in the foam material by capillarity. An adequate SH_2 quantity could be remained in the shell by regulating both the H_2 pressure and the target temperature during solidification process. The solid layer condition appears to be affected by both the exchange GHe temperature and the cooling duration. Based on the experimental results, optimum conditions are expected to realize the ideal fuel layering.

Acknowledgements

This work was partly supported by the JSPS-CAS Core-University Program in the field of "Plasma and Nuclear Fusion".

References

[1] A. Iwamoto, R. Maekawa, T. Mito, M. Okamoto, O. Motojima, M. Nakai, *et al.*, *Proceedings of Inertial Fusion Sciences and Applications 2005*, Biarritz, France, 4-9 September, 2005, p.899, EDP Sciences (2006).

[2] A. Iwamoto, R. Maekawa, T. Mito, M. Okamoto, O. Motojima, S. Sugito, *et al.*, *Fusion Eng. Des.* **81**, 1647 (2006).

[3] A. Iwamoto, R. Maekawa, T.Mito, H. Sakagami, O. Motojima, M. Nakai, et al., *Fusion Sci. Technol.* **51**(4), 753-757 (2007).

[4] J. K. Hoffer, L. R. Foreman, *Phys. Rev. Lett.* **60** (13), 1310-13 (1988).

[5] C. M. Chen, T. Norimatsu, Y. Tsuda, T. Yamanaka, S. Nakai, *J. Vac, Sci. Technol.* **A11** (3), 509-13 (1993).

Detecting the Uniformity of Polymer Foams by β-ray Technology

Zhang Lin[1], Shan Wenwen, Jia Peng, Xu jiajing,
Research Center of Laser Fusion, China Academy of Engineering Physics, Mianyang 621900

The density uniformity of the foams used as part of inertial confinement fusion targets and Z-pinch loads is critical to simulate and understand the experimental results. Usually, an average foam density has been gravimetrically determined without providing any information of the density uniformity. In this paper, a β-ray technology was introduced in order to determine the foam density uniformity. It shows that the β-ray technology can identify non-uniform density regions economically and expediently, thereby afford a new technique for process control in a foaming system. A comparison of the β-ray detecting results with the X-ray radiography results were presented.

Strictly controlling the temperature is very important for reproducibly producing uniform polymer (such as (4-methyl-1-pentene) polymer, PMP) foams during the multi-step fabrication processes. In order to take a comparison between different producing conditions, 1# and 3# were prepared by original methods (cooling down naturally in an oil bath) with d=6.4mm. 2# and 4# were prepared by modified methods (cooling down in an ice-water bath) with d=600μm. The equipment setup is composed of β-ray (^{90}Sr) source, collimation device, detector, signal amplifier, and personal computer.

Fig.1 shows the results of two cylindrical PMP foam samples (1# and 2#) with a nominal density of 40mg/cm^3. The 1# sample (d=5.0mm) is a representative of PMP foam prepared with the earlier procedure. The 2# sample (d=600μm) target image shows qualified foams with the temperature profile and other processes optimized.

The spatial resolution of 1# and 2# are 150μm and 100μm, respectively. Fig.1 (a), (b), (e) and (g) show the density distributions of 1#. The left exhibits the density distributions of 2#. Among them, (b) and (d) are 3D charts where the surface density is intuitively represented by the height. Fig.1 (e) and Fig.1 (f) are 2D charts, the grey scale stands for the face-on density. Fig.1 (g) and (h) are the statistical results from Fig.1 (e) and Fig.1 (f). Both samples exhibit a uniform density distribution along cylindrical axis [Fig.1 (a), (c)]. However, the radial density distributions are non-uniform. For 1#, the face-on density varies from 4.29mg/cm^2 in the center to 8.13mg/cm^2 towards the edge. The averaged face-on density is 6.0 mg/cm^2 and the fluctuation is 11.0%. The radial density uniformity of 2# is better, which varies from 10.70mg/cm^2 in the center to 13.98mg/cm^2 towards the edge. The averaged face-on density is 12.5mg/cm^2 and fluctuation is 4.9%. Furthermore, a skin effect appears in all of the slices. It also leads to certain density fluctuation where the foam is near to the target holder. The right part in Fig. 2 (a) towers above the other parts since it is attached to the bottom of the holder. However, there is no enhancement at the right part of Fig.1 (c) because the bottom of 2# in Fig.1 (c) was cut by machining.

The 3# and 4# samples were radiographed by a microfocus x-ray source with a 2.0 mm diameter electron spot and an 8.0 μm thick aluminum foil. From Fig. 2, the density uniformity of 4#

[1] Corresponding author: Zhang lin. PhD, condensed matter physics, e-mail:zhlmy@sina.com
Projected supported by the National Natural Science Foundation of China (NSFC No. 10574096), the Specialized Research Fund for the Doctoral Program of Higher Education of China (No. 20050610010), high energy density plasma physics national keystone laboratory foundation of China (No. 9140C6806020707).

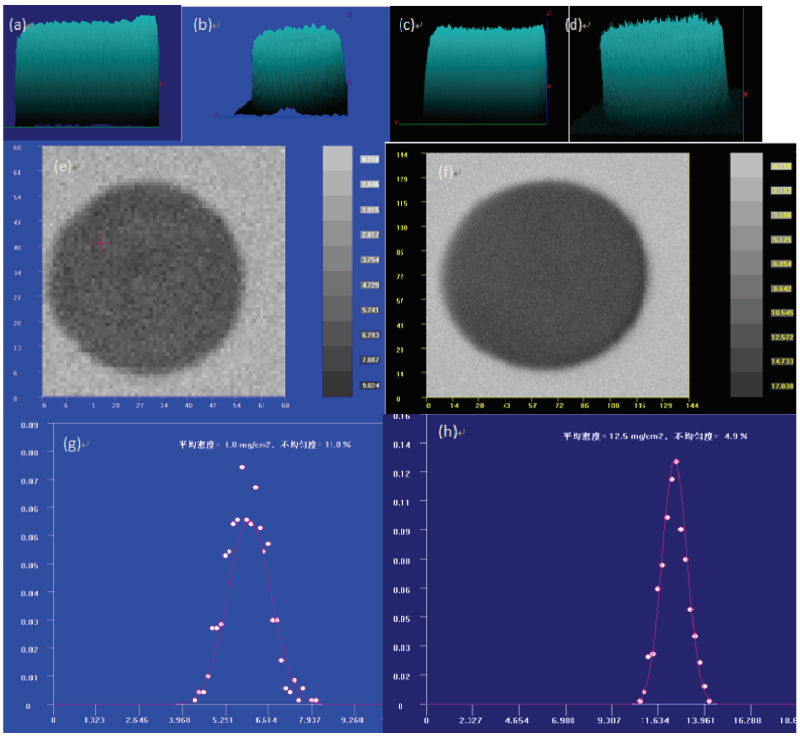

Fig. 1 density distribution along the axis and radial directions of foam samples, 1#(left) and 2# (right).

is much better than that of 3#. For 3#, the density ranges from 38.7 to 47.5mg/cm^3, the fluctuation is 8.8mg/cm^3, which is poor than the requirement of standard target (5mg/cm^3). The averaged density is 53.02mg/cm^3, the standard deviation is 6.33 mg/cm^3. As to 4#, its density ranges from 43.9 to 47.4mg/cm^3, and the fluctuation of density is 3.5mg/cm^3, which is better than the requirement of standard target. The averaged density is 45.35 mg/cm^3.The standard deviation is 0.63 mg/cm^3. If the density profile been divided into three sections: 1. less than 47.5 mg/cm^3; 2. from 47.5 mg/cm^3 to 52.5 mg/cm^3 ; and 3. greater than 52.5 mg/cm^3. The density uniformity of 4# is much more apparently: the fraction located in section 2 is 100%, while for 3#, which is only 37.44%.

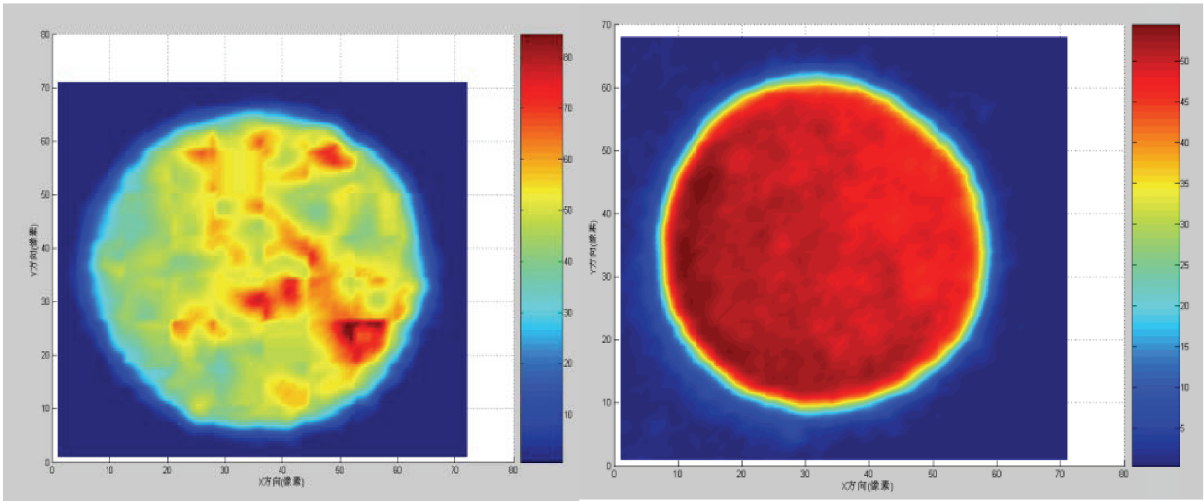

Fig.2 the face-on density distributions determined by X-ray radiograph, 3#(left) and 4# (right).

The β-ray detecting technology as a new foam uniformity characterizing method has been found constructive for the characterization of low density and ultra-low density foams. Those detecting results are significant for foam preparing experiments.

Encapsulation of Low Density Materials for the First Stage of Fast Ignition Realization Experiment (FIREX-I)

K. Nagai[a], M. Nakai[a], T. Norimatsu[a], A. Iwamoto[b], H. Azechi[a],

and K. Mima[a]

([a] Institute of Laser Engineering (ILE), Osaka University, 2-6 Yamada-oka, Suita, Osaka 565-0871, Japan, E-mail: knagai@ile.osaka-u.ac.jp; National Institute of Fusion Engineering (NIFS), 322-6 Oroshi, Toki, Gifu 509-5292, Japan)

Development of foam capsule fabrication for cryogenically cooled fuel targets is overviewed in the present paper. The fabrication development was initiated as a part of the Fast Ignition Realization Experiment (FIREX) Project at the ILE, Osaka University in the way of bilateral collaboration between Osaka University and National Institute for Fusion Science (NIFS). For the first stage of FIREX (FIREX-1), a foam cryogenic target was designed where low-density foam shells with a conical light guide will be cooled down to the cryogenic temperature and will be fueled through a narrow pipe. The required diameter and thickness of the capsule are 500 um and 20 um, respectively.[1,3] The material should be low-density plastics foam.

We have prepared such capsules using 1) new material of (phloroglucinolcarboxylic acid)/formalin resin to control kinematic viscosity of the precursor,[5] 2) phase-transfer-catalyzed gelation process to keep density matching of three phases of the emulsion.[2] 3) non-volatile silicone oil as outer oil of emulsion in order to prevent hazard halogenated hydrocarbon and flammable mineral oil.[4] (Fig.1.) The obtained foam capsule had fine structure of 180 nm (outer surface) to 220 nm (inner surface) and uniform thickness reaching to resolution limit of optical analysis (~0.5 um).(Fig.2.) A small hole was made before the solvent exchange and the drying process to prevent distortion due to volume changes. The density of dried foam was 0.29 g/cm^3. After attaching the petawatt laser guiding cone and fueling glass tube, poly([2,2]paracyclophane) was coated on the foam surface and supplied for a fueling test of cryogenic hydrogen.[6]

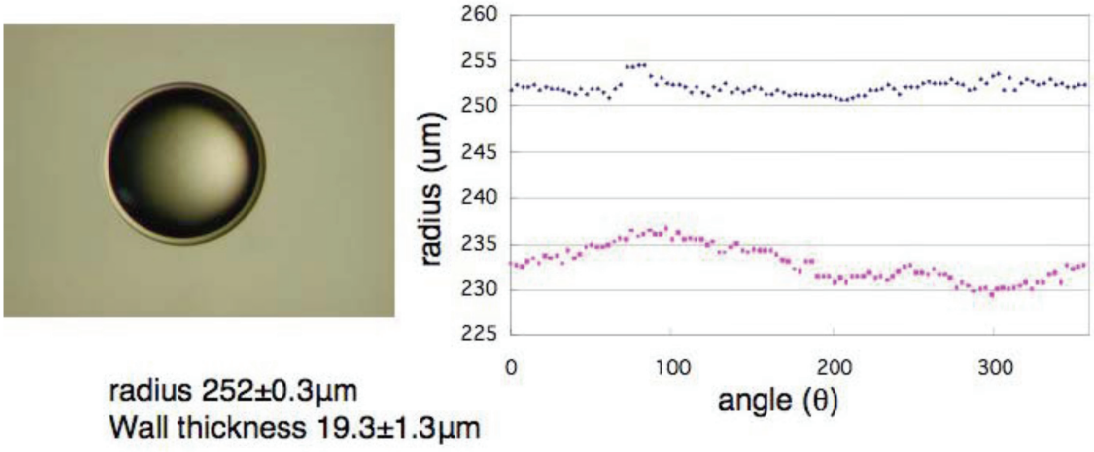

Fig. 1. An optical image of a gelated capsule (left), and its radius of depending on angle by an image analysis.

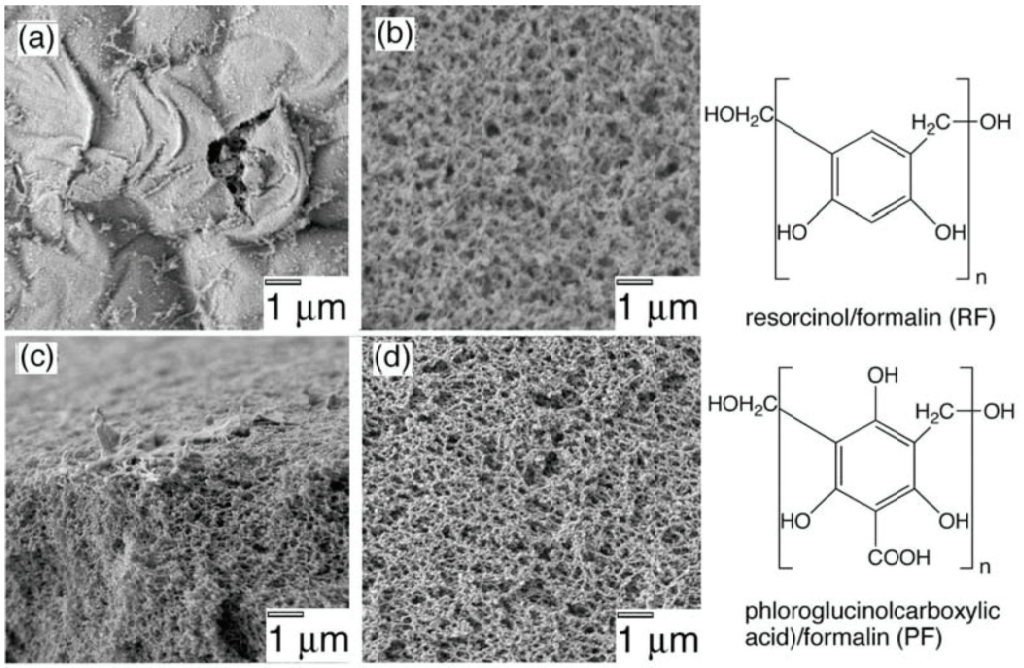

Fig. 2. SEM images a) of outer surface of RF foam obtained via 0.39 % acetic acid-catalyzed reaction and c) of outer surface of RF-PF foam obtained with 0.39 % acetic acid-catalyzed reaction. Images b) and d) show inner surface bulk morphologies of RF foam and RF-PF foam, respectively. Chemical formula of PF and RF are shown in upper-right and lower-right sides, respectively.

Acknowledgement This work was partly supported by the JSPS-CAS Core-University Program in the field of "Plasma and Nuclear Fusion".

References

[1] K. Nagai, et al., *Nucl. Fusion*, **45** (11), 1277-1283, (2005).

[2] F. Ito, et al., *Macromol. Chem. Phys.*, **206** (21), 2171-2176, (2005).

[3] T. Norimatsu, et al., *Fusion Sci. Technol.*, **49** (3), 483-499, (2006).
[4] F. Ito, et al., *Fusion Sci. Technol.*, **49** (4), 663-668, (2006).
[5] F. Ito, et al., *Jpn. J. Appl. Phys Part 2.*, **45** (11), L335-L338, (2006).
[6] A. Iwamoto, et al., *Fusion Eng. Des.*, **8**1 (2), 1647-1652, (2006).

Single Walled Carbon Nanotube–Porphyrin Nanohybrids: Novel Synthetic Donor–Acceptor Systems for Light Harvesting and Optical Limiting Materials

Zhen Guo,[a] Dongmei Ren,[a] Zhibo Liu[c], Feng Du,[b] Yongsheng Chen,[b] Jianguo Tian[c], and Jianyu Zheng, [a,*]

[a]*State Key Laboratory and Institute of Elemento-Organic Chemistry, Nankai University, Tianjin 300071, China. E-mail: jyzheng@nankai.edu.cn; Fax: +86 (22)-2350-5572; Tel: +86 (22)-2350-5572*

[b]*Center for Nanoscale Science and Technology and Key Laboratory for Functional Polymer Materials, Institute of Polymer Chemistry, College of Chemistry, Nankai University, Tianjin 300071, China.*

[c]*The Key Laboratory of Advanced Technique and Fabrication for Weak-Light Nonlinear Photonics Materials, Ministry of Education and TEDA Applied Physical School, Nankai University, Tianjin 300457, China*

Single walled carbon nanotubes (SWNTs) have attracted much attention since they were discovered by Ijima in 1993.[1] Due to the rigid rod-like structure and highly delocalized, extended π-electron systems of SWNTs, these one-dimensional nanowires have many unique mechanical and electronic properties.[2] Porphyrins are stable natural functional dyes with a large extinction coefficient in the visible light region, predictable rigid structures, and prospective electron-transfer ability. So the combination of SWNTs and porphyrins was expected to generate materials with excellent chemical and physical properties.

Recently, we have synthesized four SWNTs–porphyrin nanohybrids with different linkage modes (Figure 1, **1**–**4**).[3] The structure and morphology of these synthetic nanohybrids were fully characterized with Raman, FTIR, UV-Vis-NIR spectra as well as TGA, TEM, AFM measurements. Upon photoexcited by visible light, porphyrins attached on nanotube sidewalls act as light harvesting antenna and were excited to singlet excited state. Through photo induced electron transfer process (PET) to the electron acceptor SWNTs, the fluorescence of porphyrin was effectively quenched. The fluorescence quenching mechanism was studied by means of steady state fluorescence, time-resolved fluorescence and transient absorption measurement.

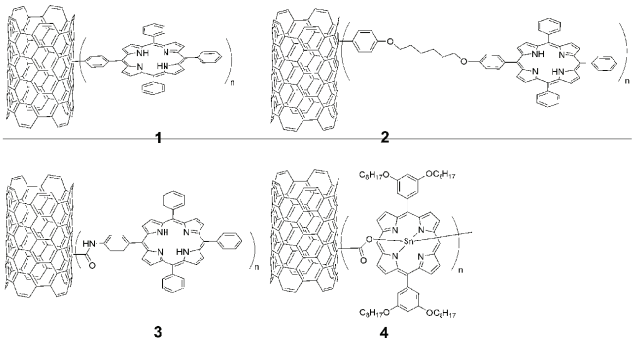

Figure 1. Schematic view of SWNTs–porphyrin nanohybrids **1**–**4**.

* We gratefully acknowledge financial support of the "973" Program (#2006CB932900) from MoST and the Natural Science Foundation of China (# 20572048, and 20421202).

Considering the donor–acceptor property of these nanohybrids in the excited state, we investigate the optical limiting behavior with nanosecond laser pulses. It is the first time for the optical limiting studies of functionalized SWNTs with reverse saturation absorption (RSA) porphyrins groups. The results indicate that these novel porphyrin functionalized SWNTs show significantly better optical limiting performance than porphyrin, SWNTs and C60 individually (Figure 2).

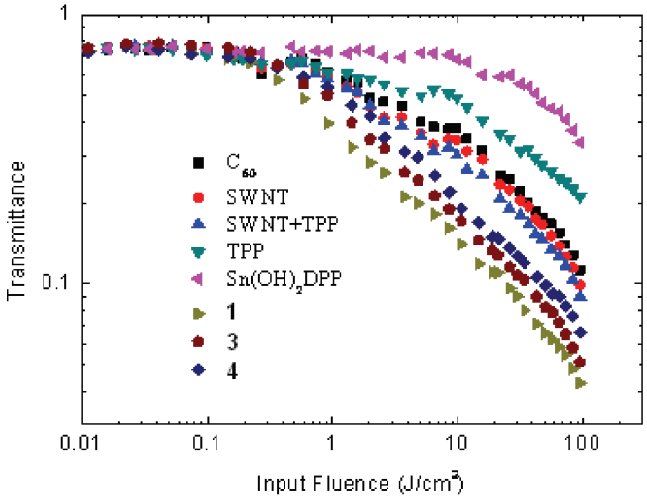

Figure 2. The output fluence *vs* input fluence of C_{60}, SWNTs, SWNTs+TPP, TPP, $Sn(OH)_2DPP$, **1**, **3**, and **4** for 5ns pulsed laser at 532nm. The linear transmittance for all of the samples was adjusted to 75%.

The fast and efficient electron transfer occurring in these donor–acceptor nanohybrids pave the way for SWNTs-based light harvesting materials in molecular photonic devices and solar energy utilization. Further studies to better understand the structure–property correlations and photovoltaic devices preparation are currently in progress.

Keywords: Single Walled Carbon Nanotubes, Light Harvesting, Electron-Transfer, Porphyrin.

References:

[1] S. Iijima and T. Ichihashi, *Nature*, **1993**, 363, 603.

[2] M.S. Dresselhaus, G. Dresselhaus, P. Avouris, *Carbon Nanotubes: Synihesis, Structure, Properties and Applications*, Springer, Berlin, **2001**.

[3] (a) Z. Guo, F. Du, D.M. Ren, Y.S. Chen, J.Y. Zheng, Z.B. Liu, and J.G. Tian, *J. Mater. Chem*, **2006**, 16, 3021; (b) D.M. Ren, Z. Guo, F. Du, Y.S. Chen and J.Y. Zheng, *J. Nanosci. Nanotech.*, **2007**, 7, 1539; (c) D.M. Ren, Z. Guo, F. Du, Z.C. Zhou, J.Y. Zheng and Y.S. Chen, *Chem. Phys. Lett.*, submitted; (d) Z. Guo, D.M. Ren, Q. Ouyang, F. Du, Y.S. Chen and J.Y. Zheng, unpublished result; (e) Z.B. Liu, J.G. Tian, Z. Guo, D.M. Ren, F. Du, J.Y. Zheng and Y.S. Chen, unpublished result.

Determination of Hydrogen Diffusion Coefficient in Hydrogen Absorption Alloy by Radioluminography

H. Homma[1], and H. Saitoh[2]

[1] *Institue of Laser Engineering, Osaka University, Suita 565-0871, Japan*

[2] *Department of Materials Science and Engineering, Muroran Institute of Technology, Muroran 050-8585, Japan*

Introduction

Imaging plate (IP) has attracted much attention as a detector [1,2] for X-rays, β-rays or electron beam because it possesses an extremely high sensitivity and wide dynamic range as about five orders for these radiation rays [3,4]. The detection of the intensity of radiation rays using IP is based on the photo-stimulated luminescence (PSL) phenomenon after irradiating the radiation rays to the IP. Thus, the experimental method to detect the radiation rays using IP is called radioluminography. By this method, two-dimensional distribution of the radioisotopes in the specimen can be observed quantitatively as the distribution of the PSL intensity. Tritium is the radioisotope of hydrogen and emits only low energy β-rays and decays into ^{3}He. Thus, we tried to apply the tritium radioluminography to determine hydrogen diffusion coefficient in materials using tritium as a radioactive tracer of hydrogen.

Experimental Procedure

$Ti_{50}Cr_{50}$ alloy in nominal composition were prepared by arc-melting in high purity argon atmosphere, and was cut to make rectangular block specimens 5 mm×5 mm×10 mm in size. Hydrogen (protium and tritium) addition into the specimen was performed by an electrochemical cathodic charging method at room temperature. The electrolyte was 0.1 kmol/m^3 NaOH aqueous solution containing tritium of 1.9 PBq/m^3. The current density and charging period were 400 A/m^2 and 4 h, respectively. Before hydrogen addition, the specimen was covered with epoxy resin except for the hydrogen added surface. The hydrogen added specimen was kept at room temperature for 24 h, and was cut along the long transverse direction, which is the hydrogen diffusion direction, to observe a cross sectional distribution of tritium. Then the specimen was put on an IP, Fujix TR2040, and the 30

radioactivity of the tritium recorded in the IP was measured by means of an IP-reader (Fujix FDL5000) as the intensity of PSL. The detail of the quantitative analysis of the surface tritium concentration was described elsewhere [5]. The PSL intensity was repeatedly measured in every 24 h to examine the time dependence of cross-sectional distribution of tritium. After the radioluminography, tritium concentration profile along the diffusion direction was measured and diffusion coefficient was determined.

Experimental Results

Figure 1 (a) shows a tritium radioluminograph of the $Ti_{50}Cr_{50}$ specimen three days passed at room temperature after the hydrogen addition, cross-sectional tritium distribution being observed. In this figure, white contrast means higher hydrogen concentration as indicated by a scale bar. The hydrogen concentration is higher at the left hand side (hydrogen added surface) and gradually decreases to the right hand side of the specimen. This shows that the tritium penetrates into the interior of the specimen. Fig. 1 (b) shows a cross-sectional tritium distribution in the $Ti_{50}Cr_{50}$ specimen nine days passed after the hydrogen addition, indicating that hydrogen penetrates more deeper into the specimen. Fig. 1 (c) shows concentration profiles of tritium in the specimens three and nine days passed after

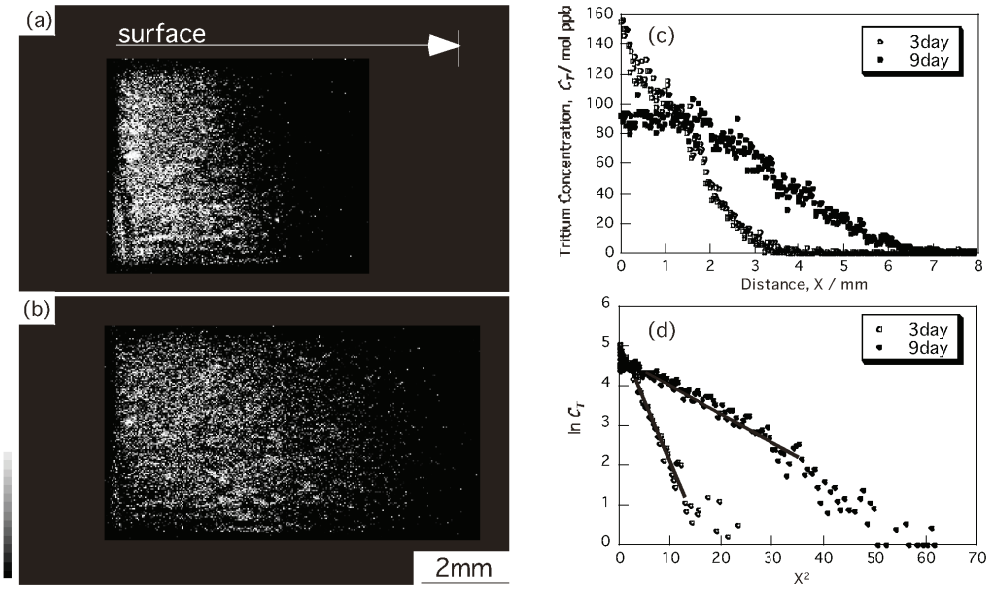

Figure 1 Tritium radioluminographs of $Ti_{50}Cr_{50}$ as-cast specimen, (a) three days and (b) nine days passed after tritium addition. (c) tritium concentration profiles on the cross-section of (a) and (b). (d) $\ln C_T$ (X, t) vs. X^2 plots of (c).

the hydrogen addition. The concentration profiles show Gaussian-like curves. However, the concentration profiles slightly deviate downward from the Gaussian curve near the hydrogen added surface of the nine days passed specimen. This is thought to be attributed that the hydrogen existed near the surface escapes to the outside the specimen.

For one-dimensional volume diffusion of a tracer from an infinitesimally thin surface layer into a sufficiently long rod, a solution of Fick's second law is given by [6]

$$C_T(X,t) = \left[M/\sqrt{\pi Dt}\right]\exp\left(-X^2/4Dt\right) \qquad (1)$$

where $C_T(X, t)$ is the concentration at the distance X from the surface after the diffusion time t, D the diffusion coefficient and M the total amount of the tracer before diffusion. Therefore, we can obtain a diffusion coefficient from the gradient of the $\ln C_T$ vs. X^2 plots. Fig. 1 (d) shows $\ln C_T$ vs. X^2 plots for the $Ti_{50}Cr_{50}$ specimen of the three days and nine days diffusion period. In this figure, the three regions are recognized, that is, the region that is affected by the backward diffusion near the hydrogen added surface, the region of volume diffusion and the region that is dropped to background. We use the region of volume diffusion for calculation of hydrogen diffusion coefficient. In Fig. 1 (d), the $\ln C_T$ vs. X^2 plots shows linearity, indicating the eq. (1) hold. From the slopes of the plots, tritium diffusion coefficients are determined. For the $Ti_{50}Cr_{50}$ specimen, tritium diffusion coefficients are 3.3×10^{-12} m^2/s and 5.1×10^{-12} m^2/s for three days and nine days of diffusion periods, respectively.

Conclusion

It is shown that the tritium radioluminography can be applicable to determine the tritium diffusion coefficient. From the cross sectional observation of hydrogen distribution, hydrogen concentration profile was measured and the hydrogen diffusion coefficient was obtained. The determined tritium diffusion coefficients in the $Ti_{50}Cr_{50}$ alloy were determined to be from 3.3 to 5.1×10^{-12} m^2/s.

Acknowledgement, This work was partly supported by the JSPS-CAS Core-University Program in the field of "Plasma and Nuclear Fusion".

Reference

[1] Y. Amemiya, 1995, J. Synchrotron Radiat., 2, 13.

[2] K. Takahashi, S. Tazaki, J. Miyahara, J. Karasawa, N. Niimura, 1996, Nucle. Instrum. Methods Phys., 377A, 119.

[3] J. Miyahara, K. Takahashi, Y. Amemiya, N. Kamiya and Y. Satou, 1986, Nucl. Instrum. Methods, A246, 572.

[4] BAS Technical Information No.2, Bio-Imaging Analyzer Group, Fuji Photo Film Co. LTD.

[5] H. Saitoh, T. Misawa, Y. Noya, T. Ohnishi :*Mater. Trans. JIM*, 40, pp.692-695, 1999.

[6] J. Crank, : *The Mathematics of Diffusion*, Clarendon Press, Oxford, 1975.

Inertial Confinement Fusion (ICF) Polystyrene Target Fabrication by a Microfluidic Device

Rong Zhu, Xiang-Wei Zhao, Zhong-Ze Gu*

State Key Laboratory of Bioelectronics, Southeast University, Nanjing, China, 210096

Target fabrication is of great significance in Inertial Confinement Fusion (ICF). How to get targets with high concentricity, high sphericity, smooth and even walls is the direction of development. Up to now, several technologies were developed to fabricate targets such as drop tower technology, interfacial polymerization technology and microencapsulation technology, among which triple-orifice droplet generator based microencapsulation technology developed by Osaka University is most promising and powerful in polymer target fabrication.[1~5] But the droplet generator is complicated in manipulation and a huge amount of regents is needed. Recently, microfluidic devices draw a great concern since the device can manipulate microfluids in microchannels, which can miniaturize and integrate the conventional chemical or phasical process on a smaller scale with high accuracy. Here, we assemblied a simple microfluidic device as illustrated in figure 1 for target fabrication.

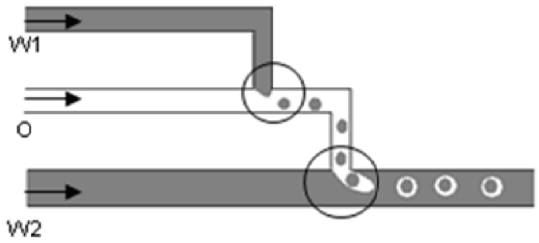

Figure 1 Schematic diagram of the microfluidic device for target fabrication. The droplet generation is highlighted in the circles.

The device was assembled with Teflon tubes and two tees. When water phase (W1) was injected to the flux of oil phase polystyrene solution (O) in another Teflon tubes through a tee, droplets were generated. And when the polystyrene solution containing water droplets pass through another tee into the flowing water, water/oil/water emulsions were generated. In general, the speed of emulsion generation is 1 per second. At the end, polystyrene capsules (Figure 2) were gained after the emulsions were solidified. And the diameters and wall thickness of the polystyrene capsules only depends on the velocity of the fluids since the tee and inner diameters of the tube are fixed as showed in Figure 3.

In conclusion, the simple microfluidic device, which can be easily assembled and manipulated, can be an alternative for polystyrene targets fabrication.

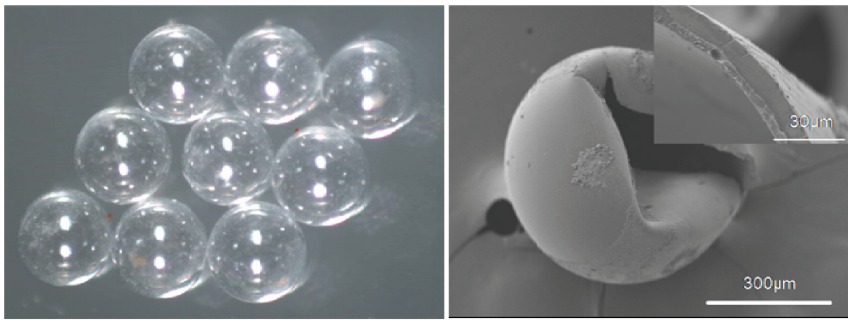

Figure 2 polystyrene targets fabricated by the microfluidic device

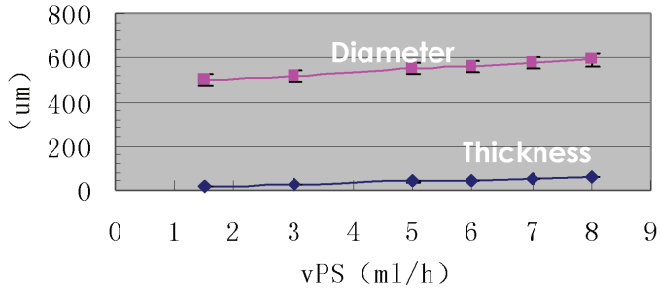

Figure 3 Relationship between capsule diameters and wall thicknesses and velocity of PS solution when the velocity of PVA solution and water were fixed at 10ml/h,0.5ml/h.

[1] Shingo Okushima, Takasi Nisisako, Toru Torii, et al. Controlled Production of Monodisperse Double Emulsions by Two-Step Droplet Breakup in Microfluidic Devices[J]. Langmuir 2004, 20, 9905-9908

[2] Zuzanna T. Cygan, Jcao T. Cabral, Kathryn L. Beers,et al. Microfluidic Platform for the Generation of Organic-Phase Microreactors[J]. Langmuir 2005, 21, 3629-3634

[3] T. Norimatsu, K. Nagai, T. Yamanaka,et al.Activities on target fabrication and injection toward laser fusion energy in Japan[J]. Fusion Engineering and Design 63~64 (2002) 587~596

[4] Keiji Nagai,Tomohiro Takaki, Takayoshi Norimatsu,et al. Fabrication of Highly Spherical Millimeter-Sized Poly(amic acid) Capsules by Removing Non-Volatile Solvent Macromol[J]. Rapid Commun. 2001, 22, 1344~1347

[5] Fuyumi ITO, Keiji NAGAI, Mitsuo NAKAI,et al. Low-Density-Plastic-Foam Capsule of Resorcinol/Formalin and (Phloroglucinolcarboxylic Acid)/Formalin Resins for Fast-Ignition Realization Experiment (FIREX) in Laser Fusion Research [J]. Japanese Journal of Applied Physics Vol. 45, No. 11, 2006, pp. L335–L338

Fabrication of NaF Films for ICF Target by Pulsed Laser Deposition

Wei-Dong Wu

Laser Fusion Research Center, China Academy of Engineering Physics

The basic principle and developing tendency of Pulse Laser Deposition and Z-scan technique were reviewed in this thesis. NaF films were successfully deposited on Si(100) substrate by Pulsed Laser Deposition. We have studied thr relationship between characters of films and esperiment parameters including laser energy density, pluse frequency and substrate temperature. According to the Z-scan theory, the experiences system called two color time-resolved and reflection Z-scan have finally been designed. The main contents of this report and conclusion are as follows:

1. The basic principles of the Pulse Laser Deposition techniques and its advantages in fabricating films have been introduced in this report, as well as discussed some recent investigations.

2. NaF films have been deposited on Si(100) substrate by Pulsed Laser Deposition at different energy density, frequency pulse and substrates temperature. The surface and structure characteristics of films have beenanalyzed by Atomic Force Microscope(AFM),X-ray diffraction (XRD),Scanning Electron Microscope(SEM) and X-ray Photoemission Spectroscopy(XPS). AFM results show that the mean square root (Rq) of films is only 0.553 nm, SEM cross-section morphology analysis indicate that the growth of films is columnar microstructure and XRD analysis reveal that the structure of films is Face Centered (fcc). the largest value of the average crystallite size (D=129.6 nm),the preferred orientation(f=0.432) and smallest value of lattice strain (ε=0.225%) are simultaneously appearing at near 400 °C. According to experiment data, the activation energy of films (48.67 kJ/mol) has been calculated.

Fabrication of Multilayered RF-PF Shells

Liqin Ge, M. Nagata, K. Nagai*, T. Norimatsu

Institute of laser engineering, Osaka University, Yamada-oka, suita 2-6, Japan

E-mail: knagai@ile.osaka-u.ac.jp

The fast-ignition concept is one of the most attractive paths to inertial fusion energy[1]. After the invention of the hollow cone/shell target geometry [2], the heating of deuterated hydrocarbon plasma was demonstrated up to a temperature corresponding to nearly 1 keV using Gekko XII and petawatt laser facilities at Osaka University [3-4]. Fuel target technology is a key issue in fast-ignition research [5].To achieve a breakeven gain, the fast-ignition realization experiment (FIREX) was designed and started with the construction of a (10 kJ)/(1 ps) laser in the first phase of FIREX (FIREX-1) and a cryogenic DT fuel target. A new cryogenic DT target for FIREX-1 is shown in Fig. 1.11) The diameter of the fuel shell is ≈500 μm, which is

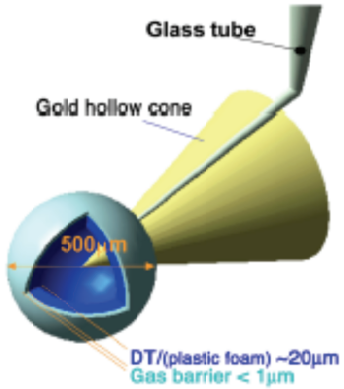

Fig.1 Schematic view of the cryogenic DT target with a plastic foam shell and a gas feeder

similar to that for a central ignition target for Gekko XII. To fabricate a uniform, non spherical solid-deuterium– tritium layer, a low-density foam supports liquid or solid fuel (≈20 μm thick) and the shell is covered with a thin (<1 μm) plastic layer. Although several kinds of foam materials have been developed for fuel targets) resorcinol/formalin (RF) resin is a candidate as the foam, because of its transparency in the visible region, which is a merit for characterizing deuterium ice uniformity.

During solvent extraction, RF shrinkage will increase its density. To circumvent the cross-linking of RF solution, we have adopted a linear copolymer composed of phloroglucinolcarboxylic acid and formaldehyde (PF) (the chemical structure of which is shown in Fig. 2), where phloroglucinolcarboxylic acid has only two reactive positions (hydrogen) in an aromatic ring; therefore, it is impossible to induce the cross-linking reaction. At present, to get a PF-RF shell with a smoother surface structure and thinner shell are a critical issue for the nuclear fusion target.

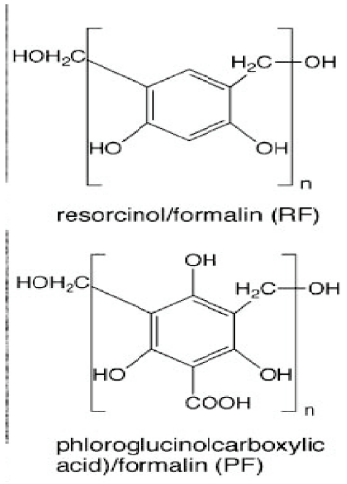

Fig.2 chemical structure of PF and RF

The electrostatic LBL method was introduced in 1991 by Decher et al.[13], and is based on the alternating adsorption of oppositely charged polyelectrolytes or particles and is one of the most frequently utilized process for the preparation of functional ultrathin films. By the LBL technique, multilayered films with well-defined thickness, composition, and structures can be prepared on solid supports. The thickness of the multilayered films can be controlled with nanoscale precision [6-8].

Layer-by-layer technique was employed to coat multilayered polyelectrolyte films on the RF-PF capsules. Four bilayers Poly (styrenesulfonate, sodium salt) (PSS, M_w 70,000) and Poly (allylamine hydrochloride) (PAH, M_w 70,000) were assembled on the shell. The obtained shell will shrank about 17% after it is dried. Surface structure of the obtained shell was studied by scanning electron microscopy (SEM) and the results show the film growth speed is affected by temperature during fabrication.

Acknowledgement: this work was partly supported by the JSPS-CAS core-university program in the field of Plasma and Nuclear Fusion.

Reference:

[1] T. Yamanaka: Institute of Laser Engineering, Osaka University, Japan (1983).

[2] M. Tabak, J. Hammer, M. E. Glinsky, W. L. Kruer, S. C. Wilks, J. Woodworth, E. M. Campbell and M. D. Perry: Phys. Plasmas 1 (1994) 1626.

[3] R. Kodama et al.: Nature 412 (2001) 798.

[4] R. Kodama et al.: Nature 418 (2002) 933.

[5] K. A. Tanaka et al.: Plasma Phys. Control. Fusion 46 (2004) B41.

[6] G. Decher, J. D. Hong and J.Schmitt: Thin Solid Films 210 (1992) 831.

[7] F. Caruso, R. Caruso and H. Möhwald: Science 282 (1998)1111.

[8] E. Donath, G. B. Sukhorukov, F. Caruso, S. A. Davis and H. Möhwald: Angew. Chem. 37 (1998) 2201.

A Simple Microfluidic Device for Generation of Colloidal Crystal Beads

Xiang-Wei Zhao, Cheng Sun, Rong Zhu, Yuan-Jin Zhao, Zhong-Ze Gu*

State Key Laboratory of Bioelectronics, Southeast University, Nanjing, China, 210096

In the last decade, droplets have been extensively used by various industries for drug development, cell encapsulation, plastic polymerization, and chemical processings. A variety of techniques are employed to generate droplets by forces of static electricity, fluidic shear and so on. In our group, a three-orifice droplet generator developed by Osaka University was used to generate droplets of colloidal solution, which turned into colloidal crystal beads after solidification in oil. The beads have a great promise in high throughput screening of biomolecules. Although the droplets prepared with the generator were stable and monodispersed, a great amount of oil was consumed in this way. Therefore, for the purpose of commercialization of the colloidal crystal beads, a more cost-effective fabrication technique with power of mass production is greatly needed. Recently, several groups have developed microfluidic technologies, in which microchannels built in elastomers, glass or silicon chips were used to control the fluids for the generation of monodispersed droplets in immiscible fluids. The fabrication of so-called microfluidic chips are highly depended on Micro Electro Mechanical Systems (MEMS), which are also cost-ineffective. And the generation is complicated by modification of the chip materials in order to avoidance clogging of the channels.

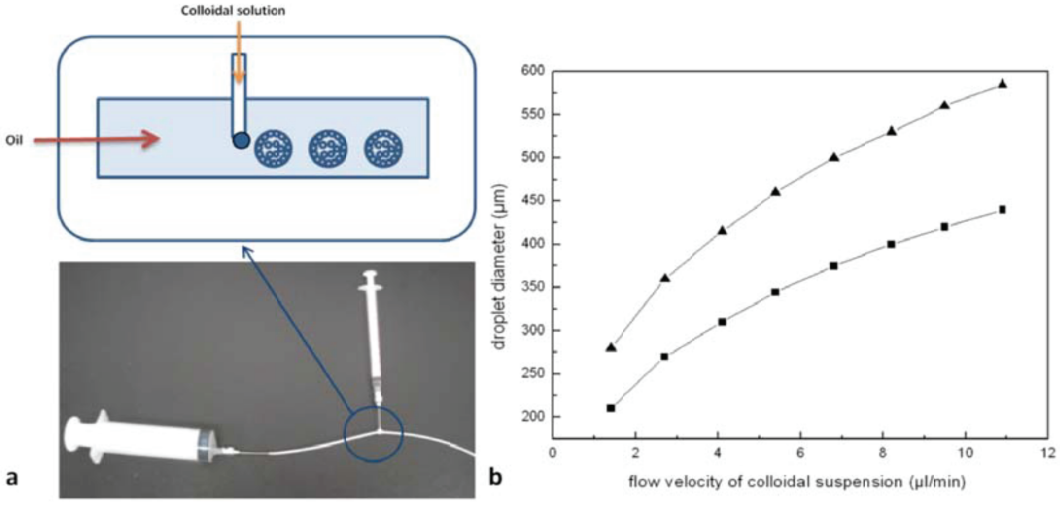

Figure 1 a, the micofluidic device used for colloidal solution droplets generation; b, the oil phase flow velocity was a constant of 50μl/min (triangular dots) and 83μl/min (quadrate dots).

Here we proposed a simple method for generation of droplets in oil as illustrated in Figure 1 a. A steel needle with inner diameter of 200 microns is penetrated into a PTFE (Poly-Tetra-Fluoro-Ethylene) tube with inner diameter of 500 microns. Silicone oil and colloidal solution of silica nanoparticles were injected to the PTFE tube by syringe pumps. Colloidal solution droplets formed on the tip of the needle are detached by the shear force of the silicon oil flux. In the device the sizes of the droplets depends on the diameter of the needle, the velocity of the oil, the velocity of the colloidal solution and the affinity between the needle and the colloidal solution. Figure 1 b, shows the relationships between the velocity of the fluidics and the droplet sizes. By this method we can get colloidal crystal beads with diameters from tens of microns to hundreds of microns.

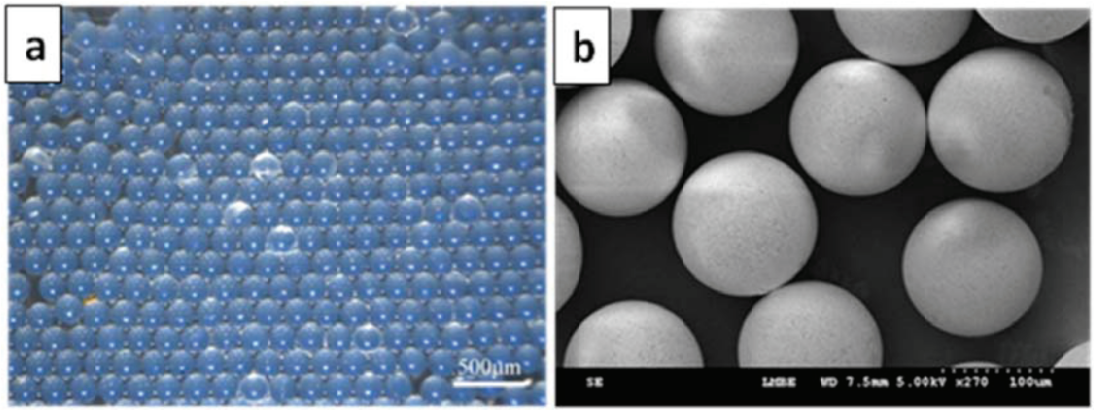

Figure 2 a, monodispersed colloidal crystal beads in ethanol; b, Scanning electronic microscope image of the colloidal crystal beads.

Regardless of its simplification, this tube and needle design yielded monodispersed droplets and hence robust colloidal crystal beads (figure 2 a and b). And the yield based on the simply microfluidic device is about 4 beads per second, which is comparable to microfluidic chips fabricated by MEMS. While the cost of the device is greatly lower than that of MEMS chips.

The Investigation on the Mechanism of Phloroglucinolcarboxylic acid/formaldehyde Gelation Process and Obvious Density Increase Before and After Extraction Drying

YANG Han, NAGAI Keiji, NAKAI Mitsuo, and NORIMATSU Takayoshi
Institute of Laser Engineering, Osaka University, Suita, Osaka, Japan
E-mail: yanghan@ile.osaka-u.ac.jp

Introduction

The fast ignition concept is one of the most attractive paths to inertial fusion energy while fuel cryogenic target [1] technology for fast ignition realization experiment (FIREX) is a key issue in this research. The target is usually spherical microcapsule, ~500μm in diameter and 20μm in shell thickness. The foam shell is used to support the fuel which consists of liquid or solid deuterium and tritium. In order to get a high gain in ignition experiment, the density of the foam shell should approach to 10mg/cc. Therefore, investigation on the foam shell materials is expected to obtain low density foam target. In this paper, one foam shell material, phloroglucinolcarboxylic acid/ formaldehyde (PF) copolymer was studied.

Experiments

In our research, spherical hollow fusion target was prepared by using the O_O /W /O_I emulsion process. The water phase solution gelates to be the shell of the capsule. PF is expected to be used as this water phase solution for shell. The gelation process of PF has been described as follows: Phloroglucinolcarboxylic acid first had addition reaction under alkaline conditions with formaldehyde to form nuclear on which the methylol groups then condense with each other to promote the growth of the nuclear. When the nucleated structure grows to a sufficient size, the coagulation starts. According to the above investigation, changing type and amount of the alkali used in the reaction can affect the nucleation process and further affect the final gelation concentration of PF. Therefore, we changed the basic condition of the reaction and the gelation concentration of PF has been reduced to 26.3mg/cc. However, after being dried by CO_2 supercritical extraction, the final density of PF foam increased to above 100mg/cc, four to five times than the concentration before extraction. The mechanism on this obvious increase may be that CO_2 used in the extraction together with small amount of no exchanged water in the gel treated the gel like acid which led to the form of subsequent bondings, such as hydrogen bonding. These additional bondings promote the shrinkage of the gel network structure which results in the decrease of the volume and the increase of the density of the dried gel. IR spectra were used to prove the existence of hydrogen bonding in the gel after extraction. Compared the IR spectrum of the dried gel after extraction with that of the gel before extraction, the additional peak around 1250cm^{-1} shows the OH---C hydrogen bonding formed in dried PF gel.

Acknowledgement, This work was partly supported by the JSPS-CAS Core-University Program in the field of "Plasma and Nuclear Fusion".

References

[1] Nagai K., Azechi H. *et al*, Nucl. Fusion., 45: 1277 (2005).
[2] F. Ito, K. Nagai, M. Nakai and T. Norimatsu, A. Nikiteniko, S. Tololonnikov, E. Koresheva, T. Fujimura, H. Azechi, and K. Mima, Jpn. J. Appl. Phys Part 2., 45 (11), L335-L338, (2006).

The Factors Affecting the Roughness of Glow Discharge Polymer (GDP) Shell

He Zhibing*, Wu Weidong, Feng Jianhong, Liu Xinghua, Ma xiaojun
Laser Fusion Research Center, China Academy of Engineering Physics

In the process of target fabrication for inertial confinement fusion (ICF) research, the fabrication of glow discharge polymer (GDP) shell is very important. How to get very smooth GDP shell is the right object in the inertial fusion capsule production. While the change of the surface roughness of GDP shell is complex. A lot of factors affect the surface roughness. In this paper, the factors affecting the surface roughness of GDP coating were investigated, such as environment cleaning, the surface roughness of PVA/PS shell, the surface of bounce pan, the fabrication parameters of GDP coating etc. The environment cleaning meant the amount of the contamination on the PVA/PS shell. The contamination would badly destroy the surface of GDP coating and made the surface rough. The transfer process of the contamination was studied and analyzed. The super-clean environment did favor for the smooth surface of GDP shell. As the substrate, the surface roughness of PVA/PS shell impact the roughness of GDP coating seriously. The different materials coating on the bounce pan had obvious effects on the roughness of GDP coating. The metal coating on the bounce pan was favor for smoothing the GDP coating. In many kinds of metal, the copper coating had the best effect on the roughness. In the fabrication parameters, the flow ratio of T_2B /H_2 and the deposition pressure were the main parameters on the roughness of GDP coating. The results indicated that the roughness increased with increasing the flow ratio of T_2B /H_2 to 0.79. After 0.79, the ratio increased that resulted in the roughness decreasing. When the ratio reached 4, the RMS roughness of the GDP coating could get to 0.97 nm. The roughness of the GDP coating decreased with increasing the deposition pressure. When the deposition pressure was at 21 Pa, the GDP coating became homogeneous and compact, and the RMS roughness was less than 1 nm.

* Corresponding author: Tel.: +86-816-2494151, Fax: +86-816-2493148
E-mail: zjuhezhibing@yahoo.com.cn

Alignment Control and Templating Process in Amphiphilic Block Copolymer Thin Film

Kaori KAMATA[1,2] and Tomokazu IYODA[2]

[1]*JST-PRESTO, 4-1-8, Hon-cho, Kawaguchi, Saitama 332-0012, Japan.*
[2]*Tokyo Institute of Technology, Chemical Resources Laboratory, 4259 Nagatsuta, Midori-Ku, Yokohama, Kanagawa 226-8503, Japan.*

Introduction

Self-organization ordering into periodic nanostructures has potential use in applications ranging from optics to microelectronics, leading to developments on bottom-up nanotechnologies. Block copolymer is one of the foremost examples due to its micro/nanophase separated structure with high scalability based on the polymer synthesis, i.e., polymer compositions. Fabrication of the block copolymer film materials with well-aligned nanostructures, however, is still challenge. External stimuli such as electric fields controlled interfacial interactions and solvent evaporation effect have been used to control the alignment in the block copolymer materials.[1] These techniques are still required to apply for various kinds of film shapes and thicknesses and to extend to the nanotemplates[2] hybridizing with electronic, magnetic, or photonic functional components. Herein, we demonstrate the electrochemical control of microdomain alignments in amphiphilic block copolymer film consisting of hydrophilic polyethylene oxide (PEO) and hydrophobic polymethacrylate with azobenzene-based liquid crystalline side-chain (PMA(Az)) as shown in **Fig. 1**. The AFM study was carried out to observe the microdomain alignments of the hexagonal nanocylinders against the substrate.

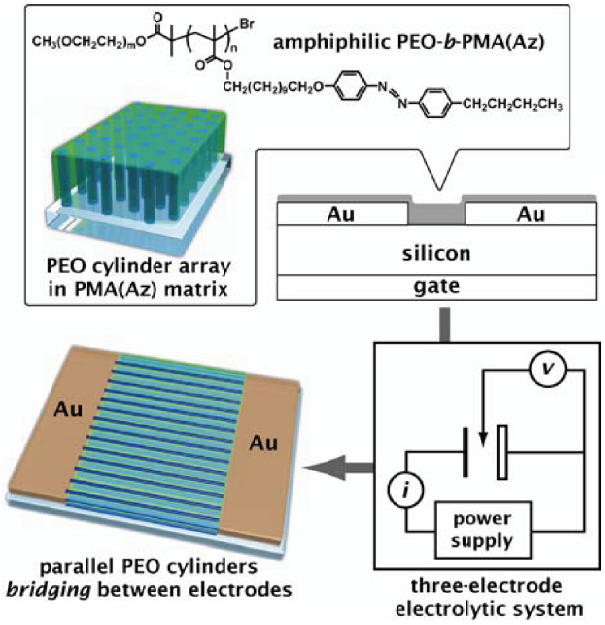

Fig. 1. Chemical structure of amphiphilic block copolymer, PEO_m-*b*-$PMA(Az)_n$ and illustration of experimental setup for alignment control of its phase-separated nanocylinder array structure.

Experimental

The diblock copolymer (m = 114, n = 47) was synthesized by a previously published procedure.[2a] A 2 wt% toluene solution of the diblock copolymer was cast onto the silicon wafer, ITO electrode, or semiconducting substrate designed for field emission transistor with 10 μm electrode gap. The resulting film was kept in an oven preheated at 140 °C for 16 hrs.

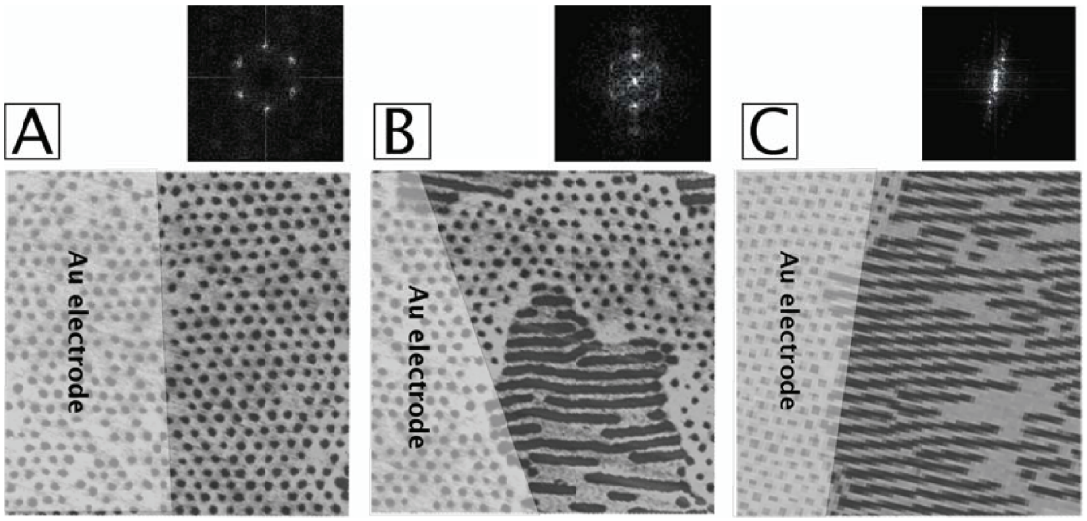

Fig. 2. AFM phase images of PEO-*b*-PMA(Az) thin film coated into the gap between Au electrodes (A) before electrochemical alignment, (B) after 5-min and (C) after 15-min application of electrochemical E-field. Scan area: 500 nm x 500 nm. The shaded areas indicate Au electrodes behind the films.

Sandwich type cell was set with the ITO glass substrate as working electrode and Teflon spacer. A 0.5 M KBr aqueous solution was injected therein and an electrolytic potential was applied in rectangular wave function mode (-1.0 V for 1 min and +1 V for 1 min) using Hokuto HZ-3000 with Pt counter electrode and Ag/AgCl reference electrode.

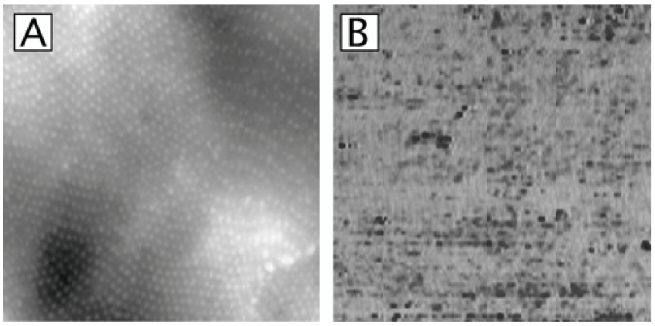

Fig. 3. (A) Tapping mode AFM height image and (B) conductive AFM image of polypyrrole nanodot array structure in PEO-b-PMA(Az) template surface. The contact mode was utilized in (B). Scan area: 1μm x 1μm.

Results and discussion

The cast film annealed above isotropic temperature overnight has shown hexagonal PEO dot pattern with a characteristic period of 20 nm. Microtome cutting has demonstrated the normal orientation of PEO cylinder microdomain to the substrate over a range of several micrometers, leading to the assignment of dot pattern in the AFM image as (001) face of the cylinder microdomain. However, a significant limitation of this technique was found as a lack of reproducibility, leading us to realize the potential of the external stimuli inducing the complete alignment.

The electrochemical treatments can be utilized to control the orientation for repeatable preparation of nanocylinderical surface patterns. The AFM observations were carried out to examine the electrochemical processing by using the thin film in Au electrode FET gap (**Fig. 2**). When the cast film was annealed at 140 ˚C 18 hrs, the cylinders were mainly laid up against a plane of the FET substrate. To this film the application of rectangular wave

function at 50 ˚C yields the cylinder orientation essentially parallel to the substrate. The surface areas corresponding to (001) face of hexagonal cylinder array, $A_{\perp}/(A_{\perp}+A_{\parallel})$, were obtained by the AFM images to estimate the effective charge passed through the film for the alignment under the potentiostatic rectangular wave mode, yielding 92 % at 0 min, 74 % at 5 min, 53 % at 10 min, 12 % at 15 min. The results were consistent with the report that the self-organized nanocylinder microdomains align parallel to the electrolytic field as the lowest energy orientation.[1b] Additionally in our system, the ionic diffusion locally induced in the vicinity of the electrode could function as making passage of hydrophilic PEO cylinder normal to the external field, leading to the control of cylinder microdomains.

Through the experimental results indicating ionic diffusion in PEO domains, we have suggested that electropolymerization in aqueous system can be versatile technique to selectively infiltrate the resulting conducting polymers into hydrophilic and ion-conductive PEO cylindrical domains. The PEO hexagonal nanodot pattern lower than the PMA(Az) matrix was morphologically changed to nanopost array structure after the electropolymerization of pyrrole (**Fig. 3a**). Since the conductive mapping with AFM contact mode depicted the hexagonal pattern similar to the electropolymerized film (**Fig. 3b**), it is quite natural to conclude that the domain-selective growth of polypyrrole was achieved from the PEO perpendicular cylinder arrays.

Conclusion

The highly aligned nanocylinders were fabricated using the cast film of PEO-*b*-PMA(Az) diblock copolymer under electrochemical E-field. It has been shown that rectangular wave function is an effective means of orientating cylinder microdomain normal to the external field. This technique could be promising candidates to tailor various cylinder orientations over areas of many square centimeters as well as decorating with conducting organic polymers and metals.

References

[1](a) A. Keller, E. Pedemonte, F. M. Willmouth, *Nature* **1970**, *225*, 538. (b) for example, T. L. Morkved, M. Lu, A. M. Urbas, E. E. Ehrichs, H. M. Jaeger, P. Mansky, T. P. Russell, *Science* **1996**, *273*, 931. (c) A. Sidorenko, I. Tokarev, S. Minko, M. Stamm, *J. Am. Chem. Soc.* **2003**, *125*, 12211.

[2](a) Y. Tian, K. Watanabe, X. Kong, T. Iyoda, *Macromolecules* **2002**, *35*, 3739. (b) J. Li, K. Kamata, T. Iyoda, *Adv. Mater.* **2007**, *19*, 1267. (c) K. Kamata, T. Iyoda, *Nanomaterials: From Research To Applications*, Chapter 5, Elsevier, 2006. (d) S. Watanabe, R. Juhiwara, M. Hada, Y. Okazaki, T. Iyoda, *Angew. Chem., Int. Ed.* **2007**, *46*, 1120. (e) S. Suzuki, K. Kamata, H. Yamauchi, T. Iyoda, *Chem. Lett.* in press.

Fabrication of Inner-surface-doped capsules for implosion experiments

Bo Li*, Sufen Chen, Zhan-wen Zhang, Xiaojun Ma
Laser Fusion Research Center, China Academy of Engineering Physics

In laser induced inertial confinement fusion (ICF) experiments, The neutron production rate depends on the final compressed fuel density and temperature which in turn depend on the degree of drive symmetry, shell integrity and shell isentropy maintained during compression. For indirectly driven spherical plastic capsules at the "Shenguang II" facility, time resolved x-ray spectroscopy of tracer dopants in the most inner surface and fuel are used to diagnose the implosion. While the argon serves as a noninvasive emission diagnostic of the electron temperature, density, and spatial profile of the fuel, the S-doped inner surface offers information about the interface between shell and fuel during the implosion.

Inner-surface-doped polystyrene capsules are prepared via emulsion encapsulation method with polystyrene sulphonate sodium(PSS) as dopant. XPS characterization indicate that inner-surface is really coverd by PSS while there is almost no observable dopant on the outer-surface. X-ray radiographs reveall that during capsule drying process, due to the surface tension, free dopant will enrich at liquid-gas interface and make a strong impact on the uniformity of dopant-layer.

Because of the small size of the doped capsules, the thickness of doped-layer is difficult to characterize. Geometrical limit introduces more problems in the application of ion beam scattering techniques. On the basis of plate experiments and AFM analysis, an approximate estimate is given, which goes to show that the thickness of doped-layer is about 10nm in our experimental condition.

* correspondence author, email: LB6711@126.com

A Simple Method to Prepare Coalesced Colloidal Crystal Film

Hua Xu, Cun Zhu, Juan Li, ZhongZe Gu*
State Key Laboratory of Bioelectronics, Southeast University, Nanjing 210096, China,

Colloidal photonic crystals, built up by periodic structures units, can generate iridescent colors of structural origin based on the Bragg diffraction of light due to their complete manipulation of the propagation of light. Many techniques have been developed to prepare colloidal crystals from silica or polymer spheres, such as sedimentation, drying of dispersions and so on. From a practical point of view, there are two main drawbacks that restrict the application of the colloidal crystal films. One is that the poor mechanical strength of the as-prepared film. The other is a tedious purification procedure (by centrifugation or filtration) needs to be carried out prior to the achievement of monodisperse spheres.

In this report, a simple, rapid method was provided to prepare the coalesced rubbery colloidal crystal films[1-2] which can improve the mechanical strength of the film. The film was composed of core/shell latex particles with a rigid core and a soft shell. The soft shells of particles in self-assembly films would merge at some temperature into a continuous elastomeric matrix in which the hard cores were still orderly embedded, so the formed coalesced films were rubbery and tough. In addition, the core/shell latex spheres used here, which have a rigid core PS and a soft shell P(MMA/EA/MAA), were prepared in one step soap-free emulsion polymerization without any further purification procedures[3].

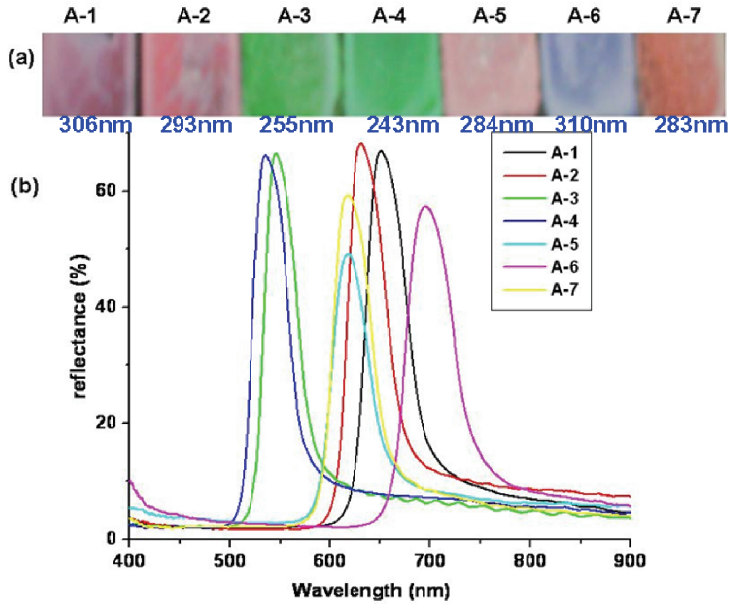

Fig. 1 (a) Photographs of as-prepared films deposited on a glass substrate. (b) Reflectance spectra of the films with sphere measured with a light incident along the normal surface ([111] direction).

The core/shell latex spheres (**A-1**～**A-7**) with different elastomeric degree of the shell were

prepared by changing the proportion of MMA/EA. The colloidal crystal films assembled from monodispersed latex spheres (**A-1**～**A-7**) all exhibited brilliant colors (Figure 1a) and strong reflectance (Figure 1b). The colors arose from light diffraction/reflectance of the colloidal arrays, indicating long range ordering of the latex spheres, which could be visualized directly by SEM (Figure 2a).

After heating at 95℃ for 4 h, the SEM image of the as-prepared films exhibited coalesced elastomeric matrix, in which the shells of adjacent spheres joined together due to melting while the hard cores were orderly embedded in it (Figure 2b). While conventional artificial opals have a matrix of air between the spheres, the matrix in coalesced opals consists of the soft shells of the latex spheres[4-5]. So the film is elastomeric and tough. However, when increasing the heating temperature to 100℃, the coalesced elastomeric films due to the flow of the latex spheres have become disordered (Figure 2c).

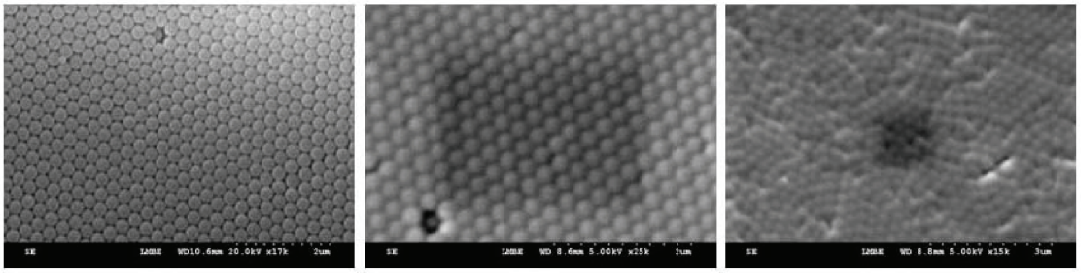

Fig. 2 SEM image of the colloidal crystal films assembled of latex spheres **A-6**; (a)at room temperature (b) heated at 95℃ for 4 h; (b) heated at 100℃ for 4 h;

Reference

【1】 T. Ruhl, G. P. Hellmann, Colloidal Crystals in Latex Films: Rubbery Opals, *Macromol. Chem. Phys.*, 202, 3502 (2001)

【2】 T. Ruhl, P. Spahn. G. P. Hellmann, Artificial opals prepared by melt compression, *Polymer*, 44, 7625 (2003).

【3】 J. X. Wang, Y. Q. Wen, H. L. Ge, Z. W. Sun, Y. M. Zheng, Y. L. Song, L. Jiang, Simple Fabrication of Full Color Colloidal Crystal Films with Tough Mechanical Strength, *Macromol. Chem. Phys.*, 207, 596 (2006)

【4】 D. Fava, et al, Order versus Disorder: Effect of Structure on the Mechanical Properties of Polymer Material, *Macromolecules,* 39, 1665 (2006).

【5】 S. Lepizzera, M. Scheer, C. Fond, T. Pith, M. Lambla, J. Lang, Coalesced Core/Shell Latex Films under Elongation Imaged by Atomic Force Microscopy, *Macromolecules*, *30,* 7953 (1997).

Ultra-low Density Foams from Ultra-high Molecular Weight Polyethylene

LUO Xuan, ZHANG Lin, DU Kai, DU Aimin
（Research Centre of Laser Fusion, CAEP, Mianyang 621900, China）

Development of the dynamic hohlraum concept as an x-ray source or inertial confinement fusion driver requires high quality low density foam components for the targets. These foams may be used to carry the current in Z-pinch plasma that implodes or they may be used to create a thermal source hold off the imploding mass from central core material. There have been many materials for low density foams, such as PMP, TMPTA, PS, PE and et al.

In this paper, it had introduced a method for fabricating the ultra-low density (<10 mg/cm^3) hydrocarbon foams from ultra-high molecular weight polyethylene （UHMW-PE） by the thermally-induced phase separation (TIPS) technique and the freeze-drying technique. Actually, the UHMW-PE has the many perfect performances, and it is pure CH material. By the Flory-Huggins theory, it had been predicted that the ultra-low density foams would be prepared from the UHMW-PE with the molecular weight more than 10^7. The fabrication procedure included of three steps: first, an entangled solution of UHMW-PE was made. Then, the solution was geled by cooling. The gel was later dried to a foam by freeze-drying technique. It had been confirmed that the morphologies and structures of these foams were mostly determined by the thermodynamics and kinetics in the procedure of phase separation and freeze drying. Finally the cylindrical, microcellular foams of 2mm diameter, 20mm length, cell sizes of 20μm, and density of 5.8mg/cm^3 had been fabricated by moulding (as shown in fig1. and fig2.), which would be used in Z-pinch experiments. By the mechanical analysis of the foams, it was obtained that the peak strain was 85% and the Young's modulus was 1700Pa.

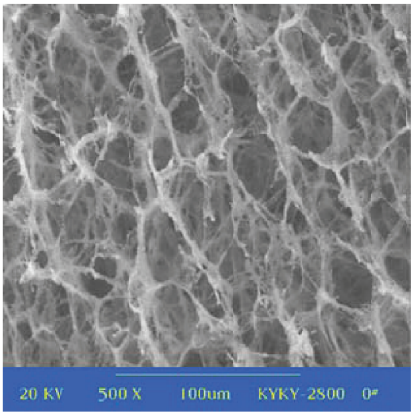

Fig1. the structures of UHMW-PE foams, 5.8mg/cm^3

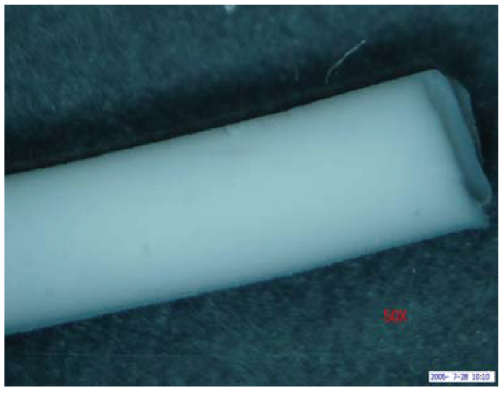

Fig2. the morphologies of UHMW-PE foams, 5.8mg g/cm^3

Fabrication of PDLC Microlenses with Microfluidic Channels

Gui-Rong Xiong, Yong-Hao Han, Guo-Zhi Han , Rong Zhu, Zhong-Ze Gu*
State Key Laboratory of Bioelectronics, Southeast University, Nanjing, China, 210096

Microlens arrays (MLA) are important optical elements which hold promise for wide applications in mini optical devices, including optical interconnections, photonic devices, integrated optics components, and optical communication systems. In order to further extend their application fields, especially in the field of microshutter array application, the lens could be also made of transmittance-tunable materials. In previous work, we ever developed a novel technique to fabricate core/shell structured microlenses with poly-*N*-isopropylacrylamide as the core material to control the transmittance through varying temperature. [1]

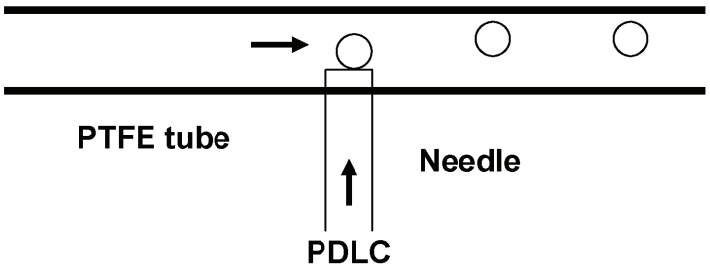

FIGURE 1 Sketch of the device for the fabrication of PDLC microlens

In this work, we upgraded our previous technique to a microfluidic device-based one and use it for fabricating polymer dispersed liquid crystals (PDLC) microball lenses. The microfluidic system could have the microball lenses to be smaller and less material-consuming. Figure 1 outlines the microfluidic device. A steel needle with inner diameter of 500 microns was penetrated into a PTFE (Poly-Tetra-Fluoro-Ethylene) tube with the same inner diameter. PDLC and PVA solution were injected respectively to the needle and the PTFE tube by syringe pumps. Herein the PDLC were prepared by mixing the uncured NOA 65 prepolymer and 5CB liquid crystal with the weight ratio of 7:1. [2] In the microfluidic system, PDLC droplets could be formed on the tip of the needle and detached by the shear force of the flowing PVA solution. The PDLC microballs were then gathered in a PVA solution filled flask and solidified under a mercury-arc lamp. These monodispersed PDLC microballs can hexagonally packed to form microlens array via a self-assembly process. Due to the phase separation of PDLC at 34 °C, the microlens array could be temperature-sensitive and could shift its optical property between the opaque and the transparent. (Figure 2)

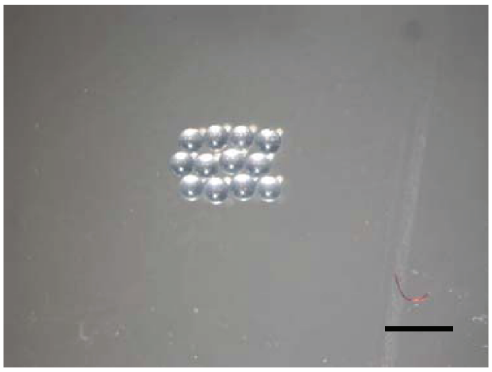

Figure 2 PDLC microlenses fabricated by microfluidic device (scale bar: 1000 μm)

[1]Han Yang, Yong-Hao Han, Xiang-Wei Zhao, Keiji Nagai,Zhong-Ze Gu. Thermal responsive arrays .Applied Physics Letters.89, 111121(2006)

[2] Hongwen Ren, Yun-Hsing Fan, and Shin-Tson Wu. Tunable Fresnel lens using nanoscale polymer-dispersed liquid crystals. Applied Physics Letters,83,1515(2003)

The Extreme Ultraviolet（EUV）Target Material Fabrication by Coaxial Electrospinning

Wei Xu, Jie Li, Qian Xu, Zhong-Ze Gu*

State Key Laboratory of Bioelectronics, Southeast University, Nanjing, China, 210096

The target material is greatly important for generating extreme ultraviolet light. Experiments and theoretical simulation have shown that both the shape of the emission light and the conversion efficiency depend on the density and the microstructure of target and nano-porous material is preferred. The problem for the target preparation turns out to be that the method should be suitable for the mass production of the low density material with the well controlled microstructure. Electrospinning is a robust method for the fabrication of EUV target.[4] The important factors such as microstructure, density, anisotropy, and mass, which have effects on the EUV transform efficiency, angular distribution, and debris, can be easily controlled.

Based on this technology, we develop a novel and simple coaxial electrospinning setup to fabricate a hollow nano-fiber film, which can reduce the density of EUV target more than the conventional electrospinning. Figure 1 shows a schematic of the coaxial electrospinning setup. One of the key components in the coaxial electrospinning setup is a compound spinneret. In our method, the coaxial spinneret as figure1 was made by two finnpipettes, one commutator of transfusion-pipe and one steel needle which is inserted into the commutator and then concentrically into a finnpipette. Another finnpipette was setted into another end of the commutator. We make use of them to develop a simple coaxial spinneret whose size can be adjusted easily by employing some parts of different size. The entrance of the inner and outer solutions are derived by transfusion-pope and the flow rates for them were controlled accurately by the precision step motor, while the output electrode from a high-voltage supply was clipped at the heel of the steel needle to charge the polymer solutions. The spinneret nipped by iron clamp is uprightly down to the aluminium foil flated on the table.

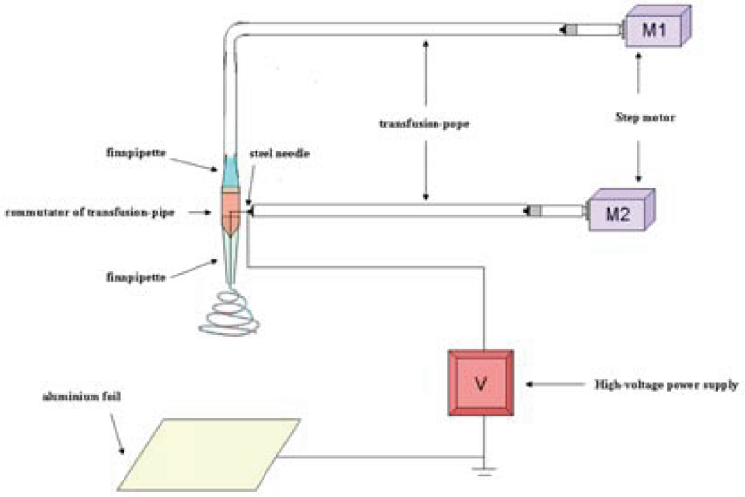

Figure 1 Schematic of the coaxial electrospunning set up

In the end, The core-shell nanofiber film can be received on the aluminium foil (Figure 2).Then the hollow nanofiber can be gained by heating or other ways.

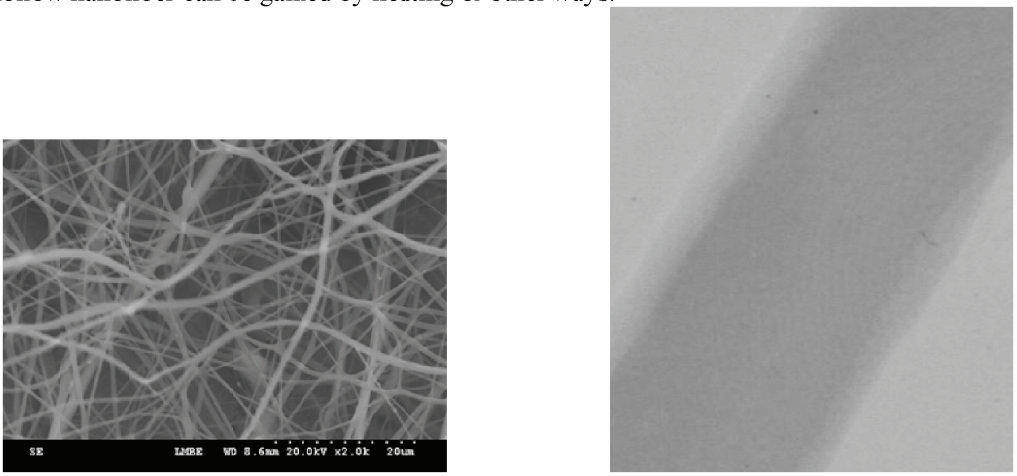

Figure 2 the SEM and TEM of coaxial electrospinning nanofiber

In conclusion, we develop a simple, controllable, low-cost device to develop low-density EUV target, which can be an alternative for polystyrene targets fabrication.

[1] Chao Pan and Zhong-Ze Gu. SnO2 target with controllable microstructure and thickness for generating extreme ultraviolet light[J]. Journal of Applied Physics 2006, 100, 016104

[2] Huang ZM, He C L , Yang A Z, et al. Encapsulating drugs in biodegradable ultrafine fibers through coaxial electrospinning[J]. J Biomed Mater Res', 2006 , 77A(1) : 1692179

[3] Ignacio G. Loscertales, Antonio Barrero, Manuel Ma´rquez, Rube´n Spretz. Electrically Forced Coaxial Nanojets for One-Step Hollow Nanofiber Design[J]. J. AM. CHEM. SOC. 2004, 126, 5376-5377

[4] Dan Li and Younan Xia*.Direct Fabrication of Composite and Ceramic Hollow Nanofibers by Electrospinning[J]. Nano Lett., Vol. 4, No. 5, 2004

Participants list

Japan

Takayoshi Norimatsu（乗松孝好）	Osaka University, Japan
Hirofumi Homma（本間啓史）	Osaka University, Japan
Akifumi Iwamoto（岩本晃史）	National Institute for Fusion Science
Hiroki Yoshida（吉田弘樹）	Gifu University, Japan
Kaori Kamata（鎌田香織）	Tokyo Institute of Technology, Japan
Yang Han （楊　菡）	Osaka University, Japan
Liqin Ge（葛　麗芹）	Osaka University, Japan
Masakatsu Murakami（村上匡且）	Osaka University, Japan
Keiji Nagai　（長井圭治）	Osaka University, Japan

China

Zhongze Gu（顾忠泽）	Southeast University,China
Xiangwei Zhao（赵祥伟）	Southeast University,China
Hongmei Wei（魏红梅）	Southeast University,China
Hua xu（徐华）	Southeast University,China
Baopin Lin（林保平 ）	Southeast University,China
Guangming Li（李光明）	Heilongjiang　University,China
Xinghua Xia（夏兴华）	Nanjing University,China
Jianyu Zheng （郑健禹）	Nankai University,China
Lin Zhang（张林）	Research Center of Laser Fusion, CAEP
Bo Li（李波）	Research Center of Laser Fusion, CAEP
Weidong Wu（吴卫东）	Research Center of Laser Fusion, CAEP
Xuan Luo（罗炫）	Research Center of Laser Fusion, CAEP
Zhibin He（何智兵）	Research Center of Laser Fusion, CAEP
Qinxue Fang（方勤学）	Office of 804 Theme
Bin Guo（郭彬）	Research Center of Laser Fusion, CAEP
Yongjian Tang （唐永建）	Research Center of Laser Fusion, CAEP